J|A|C|S ARTICLES

Published on Web 08/23/2010

A Solution- and Solid-State Investigation of Medium Effects on Charge Separation in Metastable Photomerocyanines

Dinesh G. Patel,[†] Michelle M. Paquette,[‡] Roni A. Kopelman,[†] Werner Kaminsky,[†] Michael J. Ferguson,[§] and Natia L. Frank*[,†,‡]

Department of Chemistry, University of Washington, P.O. Box 351700, Seattle, Washington 98195, Department of Chemistry, University of Victoria, P.O. Box 3065, Victoria, BC V8W 3V6, Canada, and Department of Chemistry, University of Alberta, Edmonton, AB T6G 2G2, Canada

Received January 11, 2010; E-mail: nlfrank@uvic.ca

Abstract: The effects of solution-state dielectric and intermolecular interactions on the degree of charge separation in metastable spirooxazine photomerocyanines (PMCs) is investigated. We report the first X-ray diffraction (XRD) analyses of an open form, a metastable photomerocyanine, of the spirooxazine class of photochromic molecules in two derivatives: spiro[azahomoadamantane-isoquinolinoxazine] (**1**) and spiro-[azahomoadamantane-phenanthrolinoxazine] (**2**). Using the results of XRD analysis of the open photomerocyanine forms, in conjunction with computation, solvatochromism, and solution NMR studies, we have investigated the effect of the medium on the ground-state structure of these photomerocyanines. Solvatochromism and NMR chemical shift studies of **1** and **2** support the assignment of a quinoidal structure in nonpolar solvents and a zwitterionic structure in high-polarity solvents. The effect of azahomoadamantyl substitution is explored by comparing **1** and **2** with the analogous indolyl derivatives, spiro[indoline-isoquinolinoxazine] (**3**) and spiro[indoline-phenanthrolinoxazine] (**4**) through XRD analysis of the closed spirooxazine (SO) forms, solution-state kinetic experiments, solvatochromism, and NMR studies. Longer $C_{spiro}-O$ bond lengths in the SO form and slower rates of thermal PMC → SO isomerization for the azahomoadamantyl derivatives are associated with greater zwitterionic character in the PMC form, as found in the solvatochromism studies. XRD analysis of photomerocyanines **1** and **2** indicate a greater contribution from the canonical zwitterionic resonance form relative to the quinoidal form in the solid state. Structural differences observed in two pseudopolymorphs of **2**-PMC suggest that the degree of charge-separated character is influenced by the crystal packing environment. These results provide direct structural evidence for the effects of the medium polarity on charge-separated states of photomerocyanines.

Introduction

Photochromic molecules that undergo photoisomerization between two optically and chemically distinct states[1−3] are of great interest for reversible memory photodevices,[4] optical switching elements in molecular electronics,[5] and multifunctional materials.[6−9] Of the known classes of photochromic molecules, spiropyrans and spirooxazines are distinguished by their merocyanine photoproducts which exhibit unique transition-metal binding modes,[10,11] strong nonlinear optical (NLO) responses,[4] and a tendency to organize into ordered aggregates sensitive to external electric fields.[12] The spirooxazine class in particular is technologically attractive due to its high fatigue resistance,[1] which has led to the successful incorporation of spirooxazines into light-sensitive ophthalmic lenses.[13] In addition, spirooxazines are under current investigation for optical

[†] University of Washington.
[‡] University of Victoria.
[§] University of Alberta.

(1) Bertelson, R. C. Chapter III: Photochromic Processes Involving Heterolytic Cleavage. In *Techniques of Chemistry Vol. III: Photochromism*; Brown, G. H., Ed.; Wiley-Interscience: New York, 1971.
(2) Crano, J. C.; Guglielmetti, R. J. *Organic Photochromic and Thermochromic Compounds*; Kluwer Academic Publishers: New York, 2002; Vol. 1, p 2.
(3) Dürr, H.; Bouas-Laurent, H. *Photochromism: Molecules and Systems*; Elsevier: New York, 2003.
(4) Berkovic, G.; Krongauz, V.; Weiss, V. *Chem. Rev.* **2000**, *100* (5), 1741–1753.
(5) Feringa, B. L. *Molecular Switches*; Wiley-VCH: New York, 2001.
(6) Einaga, Y.; Taguchi, M.; Li, G. M.; Akitsu, T.; Gu, Z. Z.; Sugai, T.; Sato, O. *Chem. Mater.* **2003**, *15* (1), 8–10.
(7) Taguchi, M.; Yamada, K.; Suzuki, K.; Sato, O.; Einaga, Y. *Chem. Mater.* **2005**, *17* (17), 4554–4559.
(8) Mikami, R.; Taguchi, M.; Yamada, K.; Suzuki, K.; Sato, O.; Einaga, Y. *Angew. Chem., Int. Ed.* **2004**, *43*, 6135–6139.
(9) Bénard, S.; Léaustic, A.; Rivière, E.; Yu, P.; Clément, R. *Chem. Mater.* **2001**, *13*, 3709–3716.
(10) Kume, S.; Nishihara, H. Metal-based photoswitches derived from photoisomerization. In *Struct. Bonding (Berlin)*; Springer-Verlag: Berlin, 2007; Vol. 123, pp 79−112.
(11) Kopelman, R. A.; Snyder, S. M.; Frank, N. L. *J. Am. Chem. Soc.* **2003**, *125* (45), 13684–13685.
(12) Krongauz, V. A.; Parshutkin, A. A. *Photochem. Photobiol.* **1972**, *15* (5), 503–507.
(13) Crano, J. C.; Flood, T.; Knowles, D.; Kumar, A.; Van Gemert, B. *Pure Appl. Chem.* **1996**, *68* (7), 1395–1398.
(14) Kawata, S.; Kawata, Y. *Chem. Rev.* **2000**, *100*, 1777–1788.
(15) Yuan, W. F.; Sun, L.; Tang, H. H.; Wen, Y. Q.; Jiang, G.; Huang, W.; Jiang, L.; Song, Y. L.; Tian, H.; Zhu, D. B. *Adv. Mater.* **2005**, *17* (2), 156–160.
(16) Cheng, T.; Lin, T.; Brady, R.; Wang, X. *Fibers Polym.* **2008**, *9* (5), 521–526.
(17) Mennig, M.; Fries, K.; Lindenstruth, M.; Schmidt, H. *Thin Solid Films* **1999**, *351* (1−2), 230–234.

 10.1021/ja100238h

Scheme 1

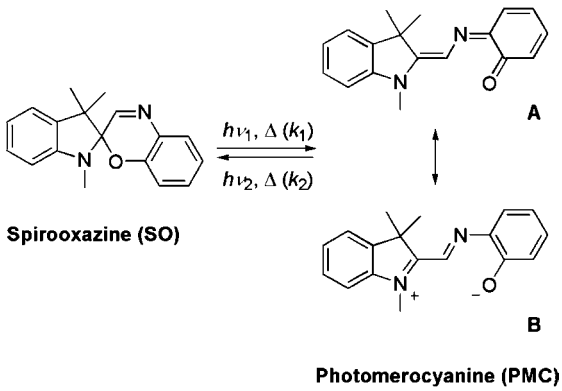

electronic devices and memories,[4,14,15] coatings,[16,17] filters,[13] displays,[4] and switches.[18,19]

Spirooxazines undergo photochemical or thermal isomerization between a spirooxazine (SO) and a photomerocyanine (PMC) form (Scheme 1). In the SO form, the azaheterocyclic and oxazine moieties are held orthogonal through a spirocyclic linkage, which leads to electronic transitions in the near-UV region ($\lambda_{max} \approx 350$ nm). UV-light-induced cleavage of the $C_{spiro}-O$ bond in the SO form leads to ring-opening and formation of the metastable PMC species, which exhibits extended conjugation through the central azomethine bridge and an intense electronic absorption at $\lambda_{max} \approx 600$ nm. Ring closure can be induced photochemically by irradiation into the low-energy PMC $\pi-\pi^*$ transition with visible light. The forward and reverse isomerization reactions can also occur thermally along the ground-state potential energy surface.[3]

The rates of thermal isomerization, photocolorability, and fatigue resistance critical for current applications of spirooxazines are controlled by subtle changes in the electronic structure of the SO and PMC forms.[2,3] While optical coatings and filters require rapid thermal relaxation,[17,20] supported by decreased stability of the PMC form, nonvolatile memories require stability of the photogenerated form.[4] The structure and reactivity of metastable photomerocyanines dictate their utility in information storage and molecular electronics applications and depend critically on the degree of charge separation and polarizability of the ground and excited states.[21−24] Our understanding of the electronic and structural factors governing spirooxazine photoisomerization dynamics and charge distribution is limited, however, by a lack of structural characterization of the metastable photomerocyanine form in the solid state. Computational and spectroscopic studies suggest that the *trans-trans-cis* (TTC) geometry of photomerocyanines is generally the most stable conformation,[25−28] while the degree of charge separation, described by the relative contributions of the quinoidal (**A**, Scheme 1) and zwitterionic (**B**, Scheme 1) resonance forms to the ground-state electronic structure, remains ambiguous. Computational studies of photochromic spirooxazine PMCs predict both zwitterionic[29,30] and quinoidal[25] ground-state structures. Solvatochromism studies suggest either a quinoidal or zwitterionic ground state depending on substituent and solvation effects.[31,32] Nucleophilic trapping studies of metastable photomerocyanines suggest a dominant zwitterionic structure in solution.[33] Structural analysis in the solid state by X-ray diffraction (XRD) through crystallization of metastable photomerocyanines has been impeded by their transient nature[34,35] and the spontaneous formation of molecular aggregates upon irradiation.[36,37] In contrast, reports of structural characterization of the metastable photomerocyanine form of the related class of spiropyrans exist, but are rare. XRD analyses of a thiospiropyran PMC form[38] and a small number of spiropyran PMC forms[39−43] suggest that spiropyran photomerocyanines with electron-withdrawing nitro and pyridinium substituents on the oxazine moiety exhibit dominant zwitterionic character. XRD analyses of two permanently open (i.e., nonphotochromic) spirooxazines indicate that the merocyanines exhibit a predominantly quinoidal structure.[44,45] To date, the structural characterization of the open form of the photochromic spirooxazine class of photochromic molecules has not been carried out by XRD analysis. Consequently, controversy persists over the relative contributions of the quinoidal and zwitterionic resonance forms to the ground-state electronic structure of spirooxazine PMCs and the explicit role of medium and substitution.[25,31,33]

Herein we investigate medium and substitution effects on the charge-separated character of photomerocyanines through a series of solution-state studies focused on bicyclic azahomoadamantyl spirooxazines. These spirooxazine derivatives exhibit

(18) Cheong, I. W.; Wang, S.; Ki, H. S.; Kim, S. H. *Curr. Appl. Phys.* **2009**, *9* (6), 1269–1271.
(19) Paquette, M. M.; Kopelman, R. A.; Beitler, E.; Frank, N. L. *Chem. Commun.* **2009**, (36), 5424–5426.
(20) Hou, L.; Schmidt, H. *Mater. Lett.* **1996**, *27* (4−5), 215–218.
(21) Marder, S. R.; Beratan, D. N.; Cheng, L.-T. *Science* **1991**, *252* (5002), 103–106.
(22) Marder, S. R.; Perry, J. W.; Bourhill, G.; Gorman, C. B.; Tiemann, B. G.; Mansour, K. *Science* **1993**, *261* (5118), 186–189.
(23) Marder, S. R.; Gorman, C. B.; Meyers, F.; Perry, J. W.; Bourhill, G.; Brédas, J.-L.; Pierce, B. M. *Science* **1994**, *265* (5172), 632–635.
(24) Teshome, A.; Kay, A. J.; Woolhouse, A. D.; Clays, K.; Asselberghs, I.; Smith, G. J. *Opt. Mater.* **2009**, *31* (4), 575–582.
(25) Nakamura, S.; Uchida, K.; Murakami, A.; Irie, M. *J. Org. Chem.* **1993**, *58* (20), 5543–5545.
(26) Perrier, A.; Maurel, F.; Perpète, E. A.; Wathelet, V.; Jacquemin, D. *J. Phys. Chem. A* **2009**, *113* (46), 13004–13012.
(27) Hobley, J.; Malatesta, V. *Phys. Chem. Chem. Phys.* **2000**, *2* (1), 57–59.
(28) Delbaere, S.; Bochu, C.; Azaroual, N.; Buntinx, G.; Vermeersch, G. *J. Chem. Soc., Perkin Trans. 2* **1997**, (8), 1499–1501.
(29) Pommier, H.; Samat, A.; Guglielmetti, R. *Mol. Cryst. Liq. Cryst. Sci. Technol., Sect. A* **1994**, *246*, 241–246.
(30) Malatesta, V.; Ranghino, G.; Romano, U.; Allegrini, P. *Int. J. Quantum Chem.* **1992**, *42* (4), 879–887.
(31) Pozzo, J.-L.; Samat, A.; Guglielmetti, R.; De Keukeleire, D. *J. Chem. Soc., Perkin Trans. 2* **1993**, (7), 1327–1332.
(32) Metelitsa, A. V.; Lokshin, V.; Micheau, J. C.; Samat, A.; Guglielmetti, R.; Minkin, V. I. *Phys. Chem. Chem. Phys.* **2002**, *4* (18), 4340–4345.
(33) Malatesta, V.; Neri, C.; Wis, M. L.; Montanari, L.; Millini, R. *J. Am. Chem. Soc.* **1997**, *119* (15), 3451–3455.
(34) Minkin, V. I. *Chem. Rev.* **2004**, *104* (5), 2751–2776.
(35) Tamai, N.; Miyasaka, H. *Chem. Rev.* **2000**, *100* (5), 1875–1890.
(36) Onai, Y.; Mamiya, M.; Kiyokawa, T.; Okuwa, K.; Kobayashi, M.; Shinohara, H.; Sato, H. *J. Phys. Chem.* **1993**, *97* (37), 9499–9505.
(37) Krongauz, V. A.; Fishman, S. N.; Goldburt, E. S. *J. Phys. Chem.* **1978**, *82* (23), 2469–2474.
(38) Hirano, M.; Osakada, K.; Nohira, H.; Miyashita, A. *J. Org. Chem.* **2002**, *67* (2), 533–540.
(39) Naumov, P.; Yu, P.; Sakurai, K. *J. Phys. Chem. A* **2008**, *112* (26), 5810–5814.
(40) Artemova, N. K.; Smirnov, V. A.; Rogachev, B. G.; Shilov, G. V.; Aldoshin, S. M. *Russ. Chem. Bull.* **2006**, *55* (9), 1605–1611.
(41) Hobley, J.; Malatesta, V.; Millini, R.; Montanari, L.; Parker, W. O. N. *Phys. Chem. Chem. Phys.* **1999**, *1* (14), 3259–3267.
(42) Aldoshin, S. M. *Russ. Chem. Rev.* **1990**, *59* (7), 663–685.
(43) Aakeröy, C. B.; Hurley, E. P.; Desper, J.; Natali, M.; Douglawi, A.; Giordani, S. *CrystEngComm* **2010**, *12* (4), 1027–1033.
(44) Laréginie, P.; Lokshin, V.; Samat, A.; Guglielmetti, R.; Pèpe, G. *J. Chem. Soc., Perkin Trans. 2* **1996**, (1), 107–111.
(45) Song, H. F.; Chen, K. C.; Tian, H. *Dyes Pigm.* **2005**, *67* (1), 1–7.

Chart 1

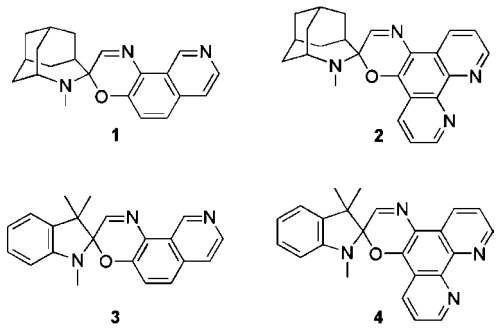

attractive properties such as crystalline-state photochromism, exceptional stability of the PMC form, high photocolorabilities, and slow thermal relaxation rates relative to their highly studied indolyl-based counterparts.[46] We report the first crystalline-state structural analysis for metastable photomerocyanines of the spirooxazine class of photochromic molecules in two derivatives: spiro[azahomoadamantane-isoquinolinoxazine] (**1**) and spiro[azahomoadamantane-phenanthrolinoxazine] (**2**) (Chart 1). The molecular structures of **1**-PMC and **2**-PMC are interpreted in the context of their relative quinoidal and zwitterionic resonance contributions. The influence of the crystalline lattice on the charge-separated character of **2**-PMC is analyzed in two crystalline pseudopolymorphs,[47] in which the degree and nature of solvation differ: **2**-PMC-I and **2**-PMC-II (a trihydrate). The molecular structures of the photomerocyanines **1**-PMC and **2**-PMC in the single crystalline state are compared with their solution-state structures as inferred from analysis of the vibrational structure and solvatochromism of the PMC $\pi-\pi^*$ absorption bands combined with ^{1}H and ^{13}C NMR studies in a wide range of solvent polarities. The effect of azahomoadamantyl substitution on charge separation and associated properties is explored by complementary studies on the analogous indolyl derivatives, spiro[indoline-isoquinolinoxazine] (**3**) and spiro[indoline-phenanthrolinoxazine] (**4**) (Chart 1). Geometrical parameters in crystal structures of **1**-SO, **3**-SO, and **4**-SO are compared within the context of relationships between oxazine geometry and photoisomerization dynamics, and are found to be consistent with that known for the wider class of spirooxazines. Solution-state isomerization kinetics and solvatochromic behavior of the azahomoadamantyl and indolyl derivatives are contrasted to examine the effect of the amine functionality on electronic structure. The stability of the metastable PMC form observed in the azahomoadamantyl derivatives correlates with the high degree of zwitterionic character. Finally, density functional theory (DFT) geometry optimizations are evaluated for their efficacy in reproducing structure−property relationships in metastable photomerocyanines, and the role of specific intermolecular interactions in both the solution and solid states found to be quite significant in these systems, leading to poor agreement between theory and experimental geometries for the PMC forms.

This work provides an analysis of structure−property relationships in spirooxazines and highlights the use of azahomoadamantyl substitution as a powerful and unexplored approach to optimizing photochromic figures of merit in spirooxazines for optical applications. Further, the direct structural evidence for the charge-separated character of metastable photomerocyanines and its sensitivity to medium polarity in both the solution and solid states is relevant to furthering our understanding of medium effects in organic systems involving charge separation. Discussions of the relative contributions of quinoidal and zwitterionic character in a wide range of organic systems have existed for some time. Investigations in spiroheterocyclics,[34] nonlinear optical materials,[48−50] electro-optic materials,[51] conjugated polymers,[52] donor−acceptor chromophores,[53] enol−keto tautomerizations in the solid state,[54,55] antiaromatic π-systems,[56] and C−O rotational barriers in esters and amides[57−60] have focused on either computation, single-crystal X-ray analysis, or solution-based studies. While it has been argued that there is a dependence on solvent polarity, direct structural evidence for medium effects in the crystalline state are valuable toward discussions of ground-state electronic structures of organics in which some degree of charge separation exists.

Results

Synthesis of Spirooxazines. The general methodology for the synthesis of spirooxazines involves the condensation of an enamine with an *o*-hydroxy-nitroso arene under dehydrating conditions.[34,61,62] The *o*-hydroxy-nitroso heterocycles required for the preparation of spirooxazines **1**−**4** were obtained from

(46) Patel, D. G.; Benedict, J. B.; Kopelman, R. A.; Frank, N. L. *Chem. Commun.* **2005**, 2208–2210.

(47) There is an ongoing debate regarding the justification and use of the term "pseudopolymorph". Nangia, A. *Cryst. Growth Des.* **2006**, *6* (1), 2–4. Bernstein, J. *Cryst. Growth Des.* **2005**, *5* (5), 1661–1662. Bernstein, J. *Polymorphism in Molecular Crystals*; Oxford University Press: Oxford, 2002; 410 pp. While the term "solvate" is an appropriate term for **2**-PMC-II, we use the term "pseudopolymorph" to compare and contrast the two structures of **2**-PMC within the discussion, and utilize the definition that "Pseudopolymorphs are solid crystalline phases of a compound formed by the same substance crystallized with different amounts or types of solvent molecules." Nangia, A. Nomenclature in crystal engineering. In *Encyclopedia of Supramolecular Chemistry*; Atwood, J. L., Steed, J. W., Eds.; Marcel Dekker: New York, 2004; Vol. 2, pp 967−972. We thank a reviewer for insightful and helpful comments with regard to this issue.

(48) Cross, G. H.; Hackman, N.-A.; Thomas, P. R.; Szablewski, M.; Pålsson, L.-O.; Bloor, D. *Opt. Mater.* **2002**, *21* (1−3), 29–37.

(49) Szablewski, M.; Thomas, P. R.; Thornton, A.; Bloor, D.; Cross, G. H.; Cole, J. M.; Howard, J. A. K.; Malagoli, M.; Meyers, F.; Brédas, J. L.; Wenseleers, W.; Goovaerts, E. *J. Am. Chem. Soc.* **1997**, *119* (13), 3144–3154.

(50) Cole, J. M.; Copley, R. C. B.; McIntyre, G. J.; Howard, J. A. K.; Szablewski, M.; Cross, G. H. *Phys. Rev. B* **2002**, *65* (12), 125107.

(51) Wang, Y. L.; Frattarelli, D. L.; Facchetti, A.; Cariati, E.; Tordin, E.; Ugo, R.; Zuccaccia, C.; Macchioni, A.; Wegener, S. L.; Stern, C. L.; Ratner, M. A.; Marks, T. J. *J. Phys. Chem. C* **2008**, *112* (21), 8005–8015.

(52) Duan, X. F.; Dudis, D. S.; Yeates, A. T. *Synth. Met.* **2001**, *116* (1−3), 285–288.

(53) Jarowski, P. D.; Wu, Y.-L.; Boudon, C.; Gisselbrecht, J.-P.; Gross, M.; Schweizer, W. B.; Diederich, F. *Org. Biomol. Chem.* **2009**, *7* (7), 1312–1322.

(54) Ogawa, K.; Harada, J.; Tamura, I.; Noda, Y. *Chem. Lett.* **2000**, (5), 528–529.

(55) Mikami, M.; Nakamura, S. *Phys. Rev. B* **2004**, *69*, 134205.

(56) Braunstein, P.; Siri, O.; Taquet, J.-P.; Rohmer, M.-M.; Bénard, M.; Welter, R. *J. Am. Chem. Soc.* **2003**, *125* (40), 12246–12256.

(57) Wiberg, K. B.; Laidig, K. E. *J. Am. Chem. Soc.* **1987**, *109* (20), 5935–5943.

(58) Wiberg, K. B.; Rablen, P. R. *J. Am. Chem. Soc.* **1995**, *117* (8), 2201–2209.

(59) Wiberg, K. B.; Rush, D. J. *J. Am. Chem. Soc.* **2001**, *123* (9), 2038–2046.

(60) Wiberg, K. B.; Rush, D. J. *J. Org. Chem.* **2002**, *67* (3), 826–830.

(61) Lokshin, V.; Samat, A.; Guglielmetti, R. *Tetrahedron* **1997**, *53* (28), 9669–9678.

(62) Chamontin, K.; Lokshin, V.; Samat, A.; Guglielmetti, R.; Dubest, R.; Aubard, J. *Dyes Pigm.* **1999**, *43*, 119–125.

Scheme 2. Synthesis of *o*-Hydroxy-Nitroso Isoquinoline and Phenanthroline Derivatives

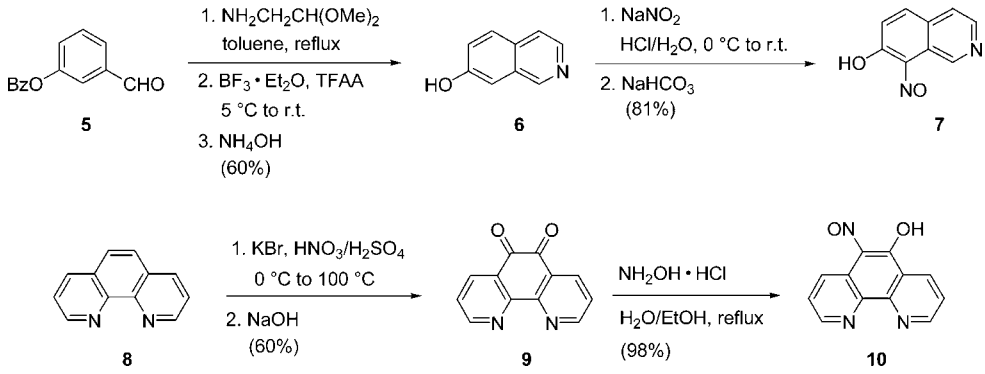

Scheme 3. Synthesis of Azahomoadamantyl Spirooxazines

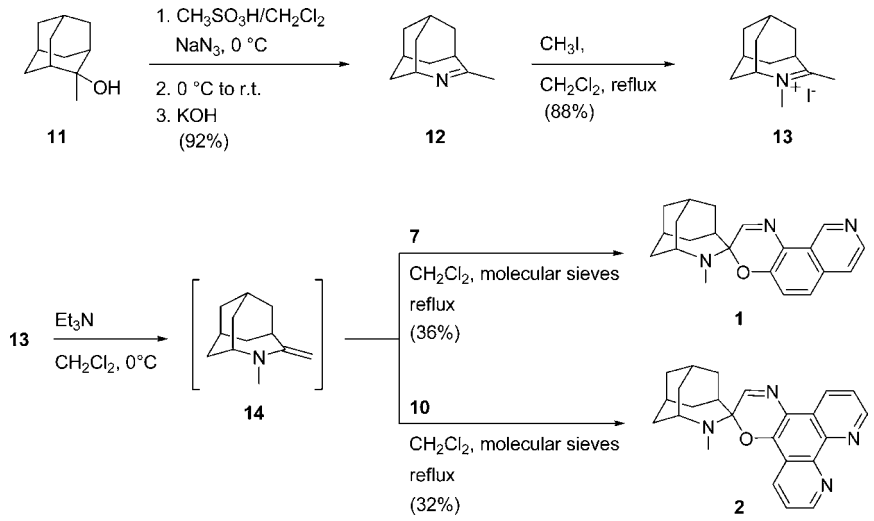

commercially available starting materials (Scheme 2).[63−66] The isoquinoline derivative (**7**) was obtained by the condensation of 3-benzyloxybenzaldehyde (**5**) with aminoacetaldehyde dimethylacetal, followed by treatment with trifluoroacetic anhydride and boron trifluoride-etherate to afford 7-hydroxyisoquinoline (**6**)[63] as a white powder in 60% yield. The nitrosylation of **6** with sodium nitrite under acidic conditions gave 7-hydroxy-8-nitrosoisoquinoline (**7**)[64] as a pale brown powder in 81% yield. The phenanthroline derivative (**10**) was obtained from 1,10-phenanthroline-5,6-dione (**9**),[65] which was prepared by the oxidation of 1,10-phenanthroline (**8**) with potassium bromide under acidic conditions to give **9** as yellow needles in 60% yield. The base-catalyzed condensation of **9** with hydroxylamine hydrochloride gave 5-hydroxy-6-nitroso-1,10-phenanthroline (**10**) as a yellow powder in 98% yield.[66]

The azahomoadamantyl spirooxazines **1** and **2** were synthesized by the condensation of the *o*-hydroxy-nitroso arenes **7** and **10**, respectively, with 4-methyl-5-methylene-4-azahomoadamantane (**14**), generated in situ by the reaction of 4,5-dimethyl-4-azahomoadamant-4-enium iodide (**13**) with triethylamine at low temperature (Scheme 3).[62] The required azahomoadamantyl iodide **13** was synthesized by the ring expansion of 2-methyladamant-2-ol (**11**) with sodium azide to give **12** as a pale yellow oil in 92% yield, followed by treatment with methyl iodide to afford **13** as a white powder in 88% yield.[67] The condensation of *o*-hydroxy-nitroso derivatives **7** and **10** with enamine **14** in dichloromethane under dehydrating conditions gave **1** and **2** as magenta and iridescent green crystalline solids in 36 and 32% yields, respectively. The indolyl derivatives **3** and **4** were obtained by the condensation of commercially available 1,3,3-trimethyl-2-methyleneindole (**15**) with *o*-hydroxy-nitroso heterocycles **7** and **10**, respectively (Scheme 4). The condensation of **15** with 7-hydroxy-8-nitrosoisoquinoline (**7**) in 2-propanol yielded spiro[indoline-isoquinolinoxazine] (**3**)

Scheme 4. Synthesis of Indolyl Spirooxazines

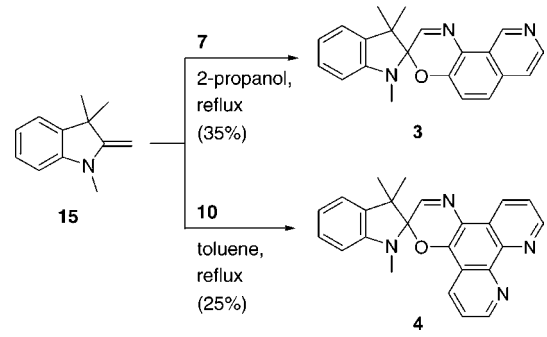

(63) Kucznierz, R.; Dickhaut, J.; Leinert, H.; von der Saal, W. *Synth. Commun.* **1999**, *29* (9), 1617–1625.
(64) Stankyavichyus, A. P.; Terent'ev, P. B.; Solov'ev, O. A. *Khim. Geterotsikl. Soedin.* **1989**, (9), 1243–1247.
(65) Paw, W.; Eisenberg, R. *Inorg. Chem.* **1997**, *36* (11), 2287–2293.
(66) Terent'ev, P. B.; Stankyavichyus, A. P. *Chem. Heterocycl. Compd.* **1988**, *24* (11), 1258–1262.
(67) Sasaki, T.; Eguchi, S.; Toi, N. *J. Org. Chem.* **1978**, *43* (20), 3810–3813.

Table 1. Thermal Equilibrium Constants,[a] K_T, % PMC Values, and Thermal Isomerization Rate Constants,[b] k_1 and k_2 [$s^{-1} \times 10^{-3}$], of **1**−**4** in Toluene, CH_3CN, and MeOH at 300 K

	toluene			CH_3CN			CH_3OH		
	K_T (% PMC)	k_1	k_2	K_T (% PMC)	k_1	k_2	K_T (% PMC)	k_1	k_2
1	<0.01 (<1)[c]	−[d]	−[d]	0.11 (10)	0.033	0.30	0.84 (46)	0.059	0.071
2	1.2 (55)	82	68	20 (95)	23	1.1	25 (96)	8.7	0.35
3	<0.01 (<1)[e]	−[d]	−[d]	<0.01 (<1)[c]	<1[f]	120[g]	<0.01 (<1)[c]	<0.1[f]	15[g]
4	0.02 (2)	4.5	230	0.07 (6)	13	190	0.07 (6)	6.5	93

[a] Determined by ^{1}H NMR; K_T = [PMC]/[SO]. [b] Determined by electronic absorption spectroscopy. [c] The concentration of the PMC form was below the limit of detection by ^{1}H NMR, although the solution was faintly colored, which indicates the presence of some concentration of PMC form with a high extinction coefficient. [d] Not evaluated. [e] The concentration of the PMC form was below the limit of detection by ^{1}H NMR, and the solution was yellow, indicating no detectable PMC form in solution. [f] Upper limit calculated with $K_T = 0.01$. [g] Calculated assuming $k_2 \gg k_1$.

as a yellow powder in 35% yield. Spiro[indoline-phenanthrolinoxazine] (**4**) was prepared by the condensation of **15** with 5-hydroxy-6-nitroso-1,10-phenanthroline (**10**) in toluene to give **4** as yellow crystals in 25% yield.[19]

Solution-State Isomerization Properties. Thermal isomerization between the SO and PMC forms of spirooxazines establishes a thermal equilibrium that can be shifted upon steady-state UV or visible irradiation to a photostationary state (Scheme 1). The thermal equilibrium constants, K_T (K_T = [PMC]/[SO]), of spirooxazines **1**−**4** were obtained in toluene, CH_3CN, and CH_3OH at 300 K from the ^{1}H NMR spectra of the compounds. This was done by calculating the ratio of the peak areas for the azomethine proton resonance of the PMC ($\delta \approx 10$ ppm) and SO ($\delta \approx 8$ ppm) forms (Table 1). The K_T values vary significantly, and range from <0.01 (<1% PMC) for the indolyl isoquinoline derivative **3** to >20 (>95% PMC) for the azahomoadamantyl phenanthroline derivative **2** in polar solvents. It is evident that the stability of the PMC isomer is greater in the phenanthroline derivatives relative to the isoquinoline derivatives and in the azahomoadamantyl derivatives relative to the indolyl derivatives. The equilibrium constants depend strongly on solvent, and become larger with increasing solvent polarity. This effect is more pronounced for the azahomoadamantyl derivatives than the indolyl derivatives. The value of K_T for **1** increases from <0.01 (<1% PMC) in toluene to 0.84 (46% PMC) in CH_3OH, and for **2**, it increases from 1.2 (55% PMC) in toluene to 25 (96% PMC) in CH_3OH. In contrast, the value of K_T only increases from 0.02 in toluene to 0.07 in CH_3CN and CH_3OH for **4**.

The photochromic behavior of compounds **1**−**4** is consistent with that of the larger class of spirooxazines and can be monitored by the intense absorption band in the visible region (>400 nm) associated solely with the PMC form. In nonpolar solvents such as pentane and toluene, the four spirooxazines are photoresponsive to UV light and exhibit an increase in the intensity of the PMC-based $\pi-\pi^*$ absorption band upon irradiation, consistent with SO → PMC conversion (Figure 1). Once a photostationary state is established with steady-state irradiation, thermal reversion to the original SO/PMC equilibrium proceeds in the absence of light, and the process of irradiation/thermal relaxation can be repeated over several photocycles. This same behavior is observed for **1**, **3**, and **4** in more polar solvents (CH_3CN and CH_3OH). For the azahomoadamantyl phenanthroline derivative **2** however, the thermal equilibrium lies far toward the PMC isomer in polar solvents, and UV irradiation leads to an irreversible decrease in the PMC band, which suggests that the PMC form is susceptible to UV-induced photodecomposition in these solvents. Visible irradiation of the azahomoadamantyl derivatives **1** and **2** leads to a decrease in the intensity of the PMC absorption band, consistent with the photoinduced conversion from the PMC form to the SO form (Figure 1). In contrast, the thermal equilibrium of the indolyl derivatives **3** and **4** lies far toward the SO form, which prevents significant visible-light-induced photoisomerization.

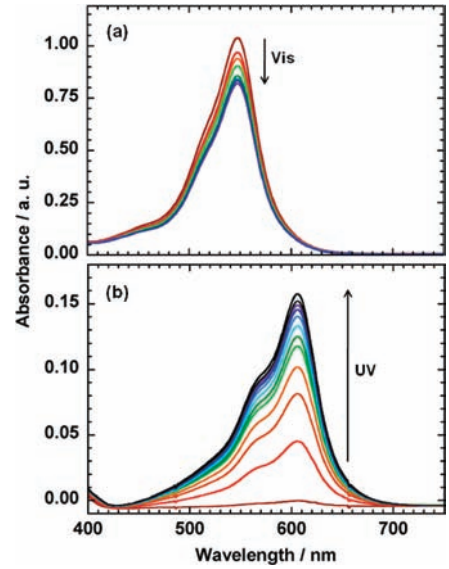

Figure 1. Electronic absorption spectra of **2** during steady-state visible irradiation (a) and of **3** during steady-state UV irradiation (b) in CH_3CN at 300 K.

The kinetics of thermal isomerization from either of the UV- or visible-light-induced photostationary states were monitored by electronic absorption spectroscopy, and the observed thermal rate constants (k_{obs}) were obtained for the PMC → SO or SO → PMC thermal isomerizations, respectively. The thermal rate constants for SO → PMC conversion (k_1) and PMC → SO conversion (k_2) (Scheme 1) were then calculated from $k_{obs} = k_1 + k_2$ and $K_T = k_1/k_2$, where K_T = [PMC]/[SO] is the equilibrium constant obtained by ^{1}H NMR spectroscopy.[1,68] These rate constants were determined in a nonpolar solvent (toluene), a moderately polar solvent (CH_3CN), and a strongly polar solvent (CH_3OH) at 300 K, and are summarized in Table 1. The values of k_1 are of the same order for the two phenanthroline derivatives **2** and **4**,[69] but are orders of magnitude lower for the isoquinoline derivatives **1** and **3**. Thus the type of substitution at the oxazine moiety clearly dominates the rates of ring-opening, where

(68) Metelitsa, A. V.; Micheau, J. C.; Voloshin, N. A.; Voloshina, E. N.; Minkin, V. I. *J. Phys. Chem. A* **2001**, *105* (37), 8417–8422.

(69) Because the k_1 value for **3** cannot be more precisely determined due to a lack of a more precise K_T value, it is not possible to compare its value for **1** and **3**. The value reported for **3** merely represents an upper limit calculated assuming $K_T = 0.01$, and it could be closer to that of **1** than it appears.

isoquinoline substitution decreases the k_1 values relative to phenanthroline substitution. The rate constants for PMC → SO isomerization (k_2) in a given solvent are sensitive to both oxazine substitution and amine functionality. The values of k_2 are 2 to 3 orders of magnitude lower for the azahomoadamantyl derivatives relative to the indolyl derivatives, and in general an order of magnitude higher for the phenanthroline derivatives relative to the isoquinoline derivatives. This suggests that the effect of amine substitution (azahomoadamantyl vs indolyl) on the rates of ring closing is substantial and more significant than the effect of substitution at the oxazine moiety. The rate constant for SO → PMC isomerization, k_1, deviates only slightly with solvent and in general remains of the same order of magnitude. The k_2 values, however, exhibit a more significant solvent dependence, and decrease with increasing solvent polarity for all of the compounds studied. This is consistent with an increase in the energy barrier to thermal ring closure in more polar solvents.

Vibrational Structure and Solvatochromism of the Electronic Absorption Spectra. The vibrational structure and solvatochromism of the PMC-based $\pi-\pi^*$ absorption band of **1**, **2**, and **4** were examined in a series of 22 solvents. The features of the absorption bands were correlated with the Dimroth−Reichardt E_T solvent polarity scale,[70] which takes into account solvation effects arising from both nonspecific (e.g., dipole−dipole, induced dipole−induced dipole, etc.) and specific (e.g., hydrogen bonding) interactions (see Supporting Information for a list of solvents used and their corresponding E_T^N values)[71] which has been found to provide reasonable correlations in solvatochromic studies of the photomerocyanines.[72,73]

Representative PMC $\pi-\pi^*$ absorption band shapes are shown in a selection of solvents for **2** and **4** in Figure 2 (also shown for **1** in the Supporting Information). All of the derivatives display a shoulder on the high-energy side of the absorption band as well as a third less prominent feature at even higher energies (between 400 and 500 nm). For the indolyl phenanthroline derivative **4**, a bathochromic shift in λ_{max} is observed with a concomitant decrease in the shoulder when going from low- to moderate-E_T^N-value solvents. However, in solvents with E_T^N values greater than ~3−4, the position and shape of the absorption band do not change significantly [Figure 2(b)]. For the azahomoadamantyl derivatives **1** and **2**, the PMC $\pi-\pi^*$ absorption bands behave similarly to that of **4** in lower E_T^N-value solvents, with a bathochromic shift in λ_{max} and decrease in shoulder intensity with increasing solvent polarity. However, in high E_T^N-value solvents, a hypsochromic shift for λ_{max} is observed along with a broadening and loss of fine structure in the absorption band [Figure 2(a)].

The PMC absorption bands for **2** and **4** were deconvoluted into three peaks with good fits using Lorentzian functions (Supporting Information). The three peaks were tentatively assigned to vibrational structure (vide infra); the lowest energy peak, labeled $\nu(1)$, accounts for 40−60% of the total peak area, the midenergy peak, labeled $\nu(2)$, accounts for 30−55% of the total peak area, and the highest energy peak, labeled $\nu(3)$, accounts for 1−15% of the total peak area. Trends are evident in both the relative peak areas and λ_{max} values for the three peaks as a function of solvent, despite a fairly high degree of scattering arising from the complex solute−solvent interactions in these photomerocyanines.

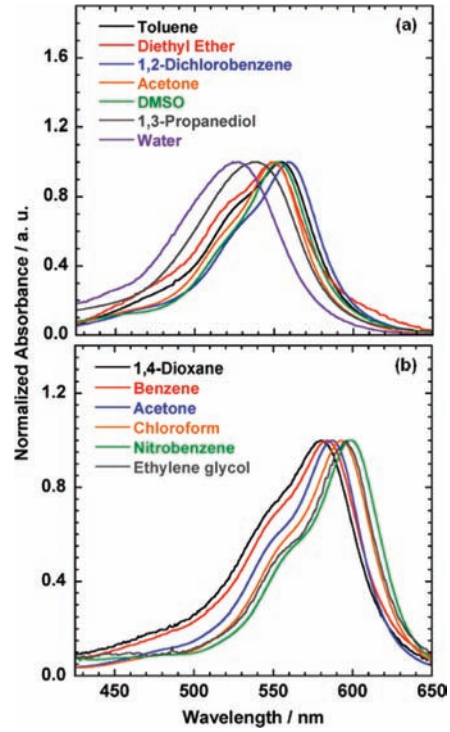

Figure 2. PMC $\pi-\pi^*$ absorption band shape at 300 K for **2** (a) and **4** (b) in a representative selection of solvents illustrating shifts in λ_{max} and changes in band structure with solvent.

The relative peak areas of $\nu(1)$, $\nu(2)$, and $\nu(3)$ for **2** and **4** are compared in Figure 3 as a function of solvent. The data were fit by locally weighted least-squares regression methods.[74] It is evident that for the azahomoadamantyl derivative **2**, the relative peak area of $\nu(1)$ increases as a function of solvent polarity until $E_T^N \approx 0.5-0.6$ before decreasing in higher polarity solvents, while the relative peak areas for $\nu(2)$ and $\nu(3)$ exhibit the opposite behavior [Figure 3(a)]. In contrast, for the indolyl derivative **4**, the relative peak area of $\nu(1)$ increases as a function of solvent until $E_T^N \approx 0.4-0.5$ before leveling off at $E_T^N \approx 0.8$, with $\nu(2)$ and $\nu(3)$ decreasing with higher solvent polarities [Figure 3(b)].

As regards the λ_{max} values of $\nu(1)-\nu(3)$ for **2** and **4**, the trends observed for $\nu(1)$ and $\nu(2)$ as a function of solvent are essentially the same, while those for $\nu(3)$ differ (Supporting Information). The λ_{max} values of the experimental $\pi-\pi^*$ absorption bands are nearly identical to the absolute values for $\nu(1)$ (Supporting Information), and are shown graphically as a function of solvent E_T^N values for **1**, **2**, and **4** in Figure 4, with the data again fit by locally weighted least-squares regression methods[74] (λ_{max} values for both the experimental and deconvoluted peaks are tabulated numerically in the Supporting Information).

For the experimental λ_{max} values, representative of the behavior of both the $\nu(1)$ and $\nu(2)$ bands, the azahomoadamantyl derivatives **1** and **2** exhibit weak solvatochromism at low (<0.2−0.3) E_T^N values and negative solvatochromism at higher (>0.3−0.4) E_T^N values. In contrast, the indolyl phenanthroline derivative **4** exhibits more pronounced positive solvatochromism in solvents with low (<0.3−0.4) E_T^N values and relatively weak solvatochromism in solvents with higher E_T^N values. In the low

(70) Reichardt, C. *Chem. Rev.* **1994**, *94* (8), 2319–2358.
(71) E_T^N is the normalized dimensionless version of Reichardt's $E_T(30)$ scale.
(72) Keum, S.-R.; Hur, M.-S.; Kazmaier, P. M.; Buncel, E. *Can. J. Chem.* **1991**, *69* (12), 1940–1947.
(73) Jacques, P. *J. Phys. Chem.* **1986**, *90* (22), 5535–5539.
(74) Cleveland, W. S. *J. Am. Stat. Assoc.* **1979**, *74* (368), 829–836.

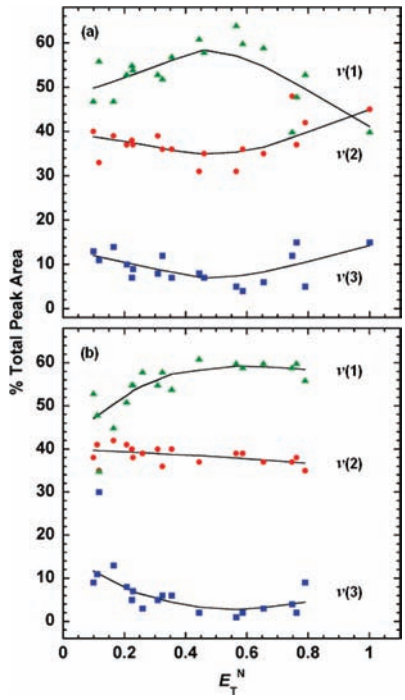

Figure 3. Relative peak areas of the three Lorentzian deconvolution peaks of the PMC $\pi-\pi^*$ absorption band, $\nu(1)$, $\nu(2)$, and $\nu(3)$, for **2** (a) and **4** (b) as a function of the Dimroth−Reichardt E_T^N solvent polarity scale at 300 K (shown as the percent of the total peak area of the sum of the deconvoluted peaks).

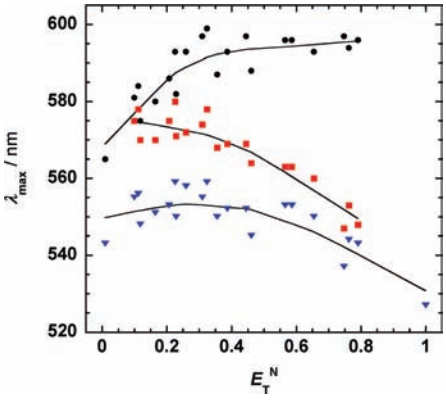

Figure 4. PMC $\pi-\pi^*$ absorption band λ_{max} values at 300 K for **1** (■), **2** (▼), and **4** (●) as a function of the Dimroth−Reichardt E_T^N solvent polarity scale.

polarity region, the greatest change in λ_{max}, $\Delta\lambda$, for **2** is 16 nm (559 nm in both 1,2-dichlorobenzene and nitrobenzene − 543 nm in pentane) vs 34 nm for **4** (599 nm in nitrobenzene − 565 nm in pentane), which evidences the more pronounced positive solvatochromism for the indolyl derivative. In the high polarity region, it is not possible to assign a positive or negative solvatochromism for **4** as the slope of the λ_{max} vs E_T^N curve is nearly zero. For **2**, however, the $\Delta\lambda$ is significant at −32 nm (527 nm in H_2O − 559 nm in 1,2-dichlorobenzene). To compare the relative negative solvatochromism of **1** and **2**, the $\Delta\lambda$ (evaluated as the difference between λ_{max} in 1,3-propanediol and 1,2-dichlorobenzene since **1** was not sufficiently soluble to obtain a spectrum in H_2O) was found to be −0.33 nm for **1** and −0.22 nm for **2**, which is consistent with greater negative solvatochromism in **1**. For both **2** and **4**, the $\nu(3)$ band exhibits

Table 2. ^1H and ^{13}C NMR Shifts of **2**-SO, **2**-PMC, **4**-SO, and **4**-PMC in a Selection of Solvents[a,b]

		2-SO		**2**-PMC				
solvent	E_T^N	H-1	H-3	H-1	H-3	C-2	C-3	C-5
toluene-d_8	0.099	2.21	7.53	2.69	10.07		123.5	
benzene-d_6	0.111	2.20	7.59	2.61	10.20			
THF-d_8	0.207	2.49	7.75	3.5	10.03	175.4	125.8	179.3
$CDCl_3$	0.259	2.48	7.71	3.51	9.98	174.6	126.2	179.8
CD_2Cl_2	0.309	2.48	7.73	3.52	10.03			
acetone-d_6	0.355	2.50	7.81	3.58	10.11			
DMSO-d_6	0.444	2.40	7.85	3.54	10.14	172.0	127.3	180.3
CD_3CN	0.460	2.44	7.75	3.51	10.12			
CD_3OD	0.762	2.45	7.75	3.62	10.16			

		4-SO		**4**-PMC				
solvent	E_T^N	H-1	H-3	H-1	H-3	C-2	C-3	C-5
toluene-d_8	0.099	2.40	7.57	2.74	10.03			
benzene-d_6	0.111	2.38	7.60	2.62	10.10			
THF-d_8	0.207	2.78	7.93	3.66	10.05	174.6		177.8
$CDCl_3$	0.259	2.76	7.83	3.65	10.01	174.5	122.5	177.4
CD_2Cl_2	0.309	2.78	7.87	3.70	10.06			
acetone-d_6	0.355	2.80	7.99	3.75	10.10			
DMSO-d_6	0.444	2.71	8.03	3.72	10.08		122.3	
CD_3CN	0.460	2.74	7.91	3.64	10.06			
CD_3OD	0.762	2.76	7.95	3.80	10.14			

[a] Spectra acquired at 300 K. [b] See Figures 5 and 7 for atom numbering.

negative solvatochromism over the full range of solvent polarities (Supporting Information).

^1H and ^{13}C NMR Spectroscopy. ^1H and ^{13}C NMR studies were performed on **2** and **4** in a range of solvents to obtain additional spectroscopic evidence for the molecular structures of the PMC form as a function of solvent polarity. Experimental ^1H NMR spectra of **2** and **4** were obtained in eight solvents ranging in polarity from toluene-d_8 to CD_3OD. ^{13}C NMR spectra were obtained in toluene-d_8, THF-d_8, $CDCl_3$, and DMSO-d_6. Experimental ^1H NMR resonances were assigned on the basis of coupling constants and 2D correlation spectroscopy. Experimental ^{13}C NMR shifts were assigned on the basis of $^1H-^{13}C$ correlation spectroscopy for all CH, CH_2, and CH_3 signals, but were assigned on the basis of the calculations for the quaternary signals. Experimental ^1H and ^{13}C NMR shifts are given in Table 2. A significant downfield shift from ∼2.7 ppm in toluene-d_8/benzene-d_6 ($E_T^N \approx 0.1$) to ∼3.6 ppm in solvents ranging from THF-d_8 to methanol-d_4 ($E_T^N \approx 0.2-0.8$) is observed for the *N*-methyl (H-1) resonance of both **2**-PMC and **4**-PMC (see Figures 5 and 7 for atom numbering). As this change is greater than that expected due to solvent effects alone (0.3−0.4 ppm for **2**-SO and **4**-SO), this may indicate a change in molecular structure upon going from very low to moderate/high polarity solvents. In contrast, the azomethine (H-3) resonance does not shift significantly with solvent polarity for **2**-PMC and **4**-PMC. The experimental ^{13}C NMR signals of **2**-PMC and **4**-PMC exhibit shifts with solvent polarity that differ slightly between the two structures. For **2**-PMC, a slight upfield shift is observed for C-2 with increasing solvent polarity (175 ppm in THF vs 172 in DMSO), with subtle downfield shifts observed at C-3. No apparent shift in C-5 is observed with changes in solvent polarity. For **4**-PMC, there is essentially no change in ^{13}C NMR shifts for C-2, C-3, and C-5 as a function of solvent polarity, although experimental values were only obtained in a narrow range of solvent polarities for this derivative. Chemical shifts were obtained in the most complete series of solvent polarities for the C-3 signal of **2**-PMC. In this case, the slight shifts

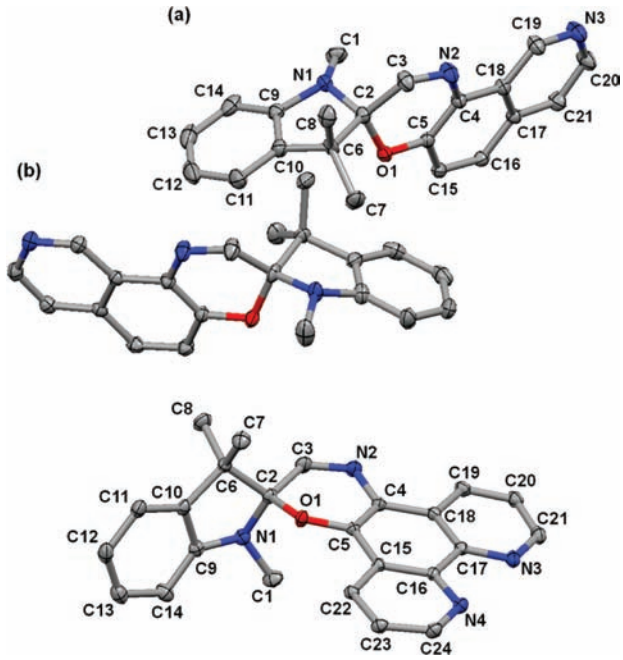

Figure 5. Molecular structures of spirooxazines **3**-SO (top) and **4**-SO (bottom) with thermal ellipsoids shown at the 50% probability level. Disorder in **3**-SO is omitted for clarity (Supporting Information).

observed may be due to a combination of subtle changes in molecular structure and specific solvation effects.

Computational NMR shift correlations are known to reproduce experimental shifts with high accuracies.[75] Theoretical NMR shifts were calculated for model quinoidal (**A**) and zwitterionic (**B**) geometries of **2**-PMC and **4**-PMC as a function of solvent in order to predict the chemical shifts of the canonical forms at their structural limits. Theoretical NMR shifts of the canonical forms were calculated using the GIAO method at the DFT/B3LYP level of theory with the 6-31G(d,p) basis set and the IEFPCM solvation model (for toluene, $CHCl_3$, and DMSO) as implemented in Gaussian 03. The agreement of the predicted chemical shifts with experiment was evaluated for **4**-SO and corrected for systematic error (Supporting Information). Significant downfield shifts of ~0.3 and ~1.5 ppm are predicted for the *N*-methyl (H-1) and azomethine (H-3) ^{1}H resonances, respectively, and downfield shifts of 10−15 ppm are predicted for the C-2, C-3, and C-5 ^{13}C resonances upon formation of a zwitterionic structure from the quinoidal form (Supporting Information). The changes in chemical shift for forms **A** and **B** as a function of solvent in **2**-PMC and **4**-PMC suggest downfield shifts as a function of increasing solvent polarity.

Comparison of experimental shifts to theoretical shifts may be useful in estimating absolute structures of **2**-PMC and **4**-PMC in solution. In both compounds, the H-1 ^{1}H NMR resonance is more upfield than that predicted for the quinoidal form (**A**) in low polarity solvents (δ_{theor} 2.79 ppm for **2**-PMC/toluene, Supporting Information) and more downfield than that predicted for the zwitterionic form (**B**) in high polarity solvents (δ_{theor} 3.26 ppm for **2**-PMC/DMSO, Supporting Information). This suggests that both **2**-PMC and **4**-PMC evolve from a quinoidal to zwitterionic structure with increasing solvent polarity. The remainder of the theoretical chemical shifts for **2**-PMC (H-3, C-2, C-3, and C-5) are all intermediate between those predicted for limiting quinoidal and zwitterionic structures, with slightly more zwitterionic character predicted. For **4**-PMC, however, the experimental H-3 shift (10.0−10.1 ppm) falls much closer to that predicted for the model quinoidal form **A** (9.9−10.1 ppm) than the zwitterionic form **B** (11.3−11.5 ppm). As regards the ^{13}C shifts for **4**-PMC, the C-2 and C-5 shifts are similarly closer to those expected for form **B**, though the shifts for C-3 are ~5 ppm more upfield than for **2**-PMC, which suggests a more quinoidal structure for this species. Caution in interpretation of the absolute theoretical chemical shift values (δ_{theor}) is necessary as the single point geometries may not be minima on the potential energy surface surface. In addition, structural effects such as methyl group free rotation and specific solvent effects are not accounted for by the computations. Nevertheless, the overall direction and trends in NMR chemical shifts suggest a more zwitterionic structure for 2-PMC relative to 4-PMC and mirror the structural changes of the PMC with increasing polarity toward a more zwitterionic structure.

X-ray Diffraction Analysis of the Spirooxazine Forms. The X-ray structural analysis of **1**-SO has been previously reported in the context of its crystalline-state photoreactivity.[46] Yellow prisms of **3**-SO and **4**-SO suitable for X-ray analysis were obtained by the slow evaporation of ethyl acetate (see ref 76 for crystal data and refinement parameters). Spirooxazine **3**-SO crystallized in the triclinic $P\bar{1}$ space group with dimers of two crystallographically independent molecules [defined as **3**-SO(a) and **3**-SO(b)] making up the unit cell ($Z = 4$). The crystal structure of **3**-SO exhibits disorder at the indolyl moiety resulting from a mixture of (*R*) and (*S*) enantiomers in the crystalline lattice (Supporting Information). Spirooxazine **4**-SO crystallized in the monoclinic $P2_1/c$ space group with four molecules in the unit cell. Packing interactions for both spirooxazines involve primarily intermolecular $\pi-\pi$ edge-to-face interactions between the orthogonal indoline and heteroaromatics in addition to weak π-stacking interactions between the heteroaromatics. No significant close contacts were noted. Packing views for **3**-SO and **4**-SO are provided in the Supporting Information.

Geometrical parameters of interest for the closed forms relevant to the kinetics and thermodynamics of isomerization include the degree of planarity of the oxazine ring, the $C_{spiro}-O$ bond length, and the degree of planarity about the amine nitrogen. The structures for **3**-SO and **4**-SO are shown in Figure 5, and selected geometric parameters for **1**-SO,[46] **3**-SO, **4**-SO, as well as the known spiro[azahomoadamantane-naphthoxazine]

(75) Bagno, A.; Rastrelli, F.; Saielli, G. *Chem.—Eur. J.* **2006**, *12* (21), 5514–5525.

(76) **1-SO.** Formula: $C_{21}H_{23}N_3O$. FW: 333.42 g mol^{-1}. Crystal system: monoclinic. Space group: $P2_1/c$. *a*: 6.6340(2) Å. *b*: 15.3270(4) Å. *c*: 16.2050(4) Å. β: 100.5580(12)°. *V*: 1619.82(9) Å^3. *Z*: 4. ρ_{calc}: 1.367 mg mm^{-3}. μ: 0.086 mm^{-1}. *T*: 130(2) K. ρ: 0.71073 Å. R_1: 0.0365. wR_2: 0.1038. $R_1 = \sum||F_o| - |F_c||/\sum|F_o|$; $wR_2 = [\sum w(F_o^2 - F_c^2)^2/\sum w(F_o^2)]^{1/2}$; $w = [\sigma^2(F_o^2) + (0.0655P)^2 + 0.3377P]^{-1}$ where $P = [F_o^2 + 2F_c^2]/3$). **3-SO.** Formula: $C_{21}H_{19}N_3O$. FW: 329.39 g mol^{-1}. Crystal system: triclinic. Space group: $P\bar{1}$. *a*: 11.0123(6) Å. *b*: 11.1746(6) Å. *c*: 14.6641(8) Å. α: 72.493(3)°. β: 89.767(3)°. ρ: 83.308(3)°. *V*: 1708.31(16) Å^3. *Z*: 4. ρ_{calc}: 1.281 mg mm^{-3}. μ: 0.081 mm^{-1}. *T*: 100(2) K. ρ: 0.71073 Å. R_1: 0.0507. wR_2: 0.1273. $R_1 = \sum||F_o| - |F_c||/\sum|F_o|$; $wR_2 = [\sum w(F_o^2 - F_c^2)^2/\sum w(F_o^2)]^{1/2}$; $w = [\sigma^2(F_o^2) + (0.0589P)^2 + 0.0199P]^{-1}$ where $P = [F_o^2 + 2F_c^2]/3$). **4-SO.** Formula: $C_{24}H_{20}N_4O$. FW: 380.44 g mol^{-1}. Crystal system: monoclinic. Space group: $P2_1/c$. *a*: 14.5008(5) Å. *b*: 8.9511(3) Å. *c*: 14.8771(6) Å. β: 107.092(2)°. *V*: 1845.73(12) Å^3. *Z*: 4. ρ_{calc}: 1.369 mg mm^{-3}. μ: 0.087 mm^{-1}. *T*: 100(2) K. ρ: 0.71073 Å. R_1: 0.0450. wR_2: 0.1236. $R_1 = \sum||F_o| - |F_c||/\sum|F_o|$; $wR_2 = [\sum w(F_o^2 - F_c^2)^2/\sum w(F_o^2)]^{1/2}$; $w = [\sigma^2(F_o^2) + (0.077P)^2 + 0.3835P]^{-1}$ where $P = [F_o^2 + 2F_c^2]/3$).

Table 3. Selected Geometric Parameters [Å, deg] for the Closed Forms of Azahomoadamantyl and Indolyl Spirooxazines[a]

	1-SO[b]	**16**-SO[c]	**3**-SO(a)[d]	**3**-SO(b)	**4**-SO	**17**-SO[e]
C(1)−N(1)	1.463(2)	1.454(1)	1.441(6)	1.448(3)	1.4610(11)	1.442(4)
N(1)−C(2)	1.431(2)	1.4311(8)	1.439(7)	1.454(4)	1.4454(11)	1.436(3)
C(2)−O(1)	1.490(2)	1.4767(7)	1.4585(16)	1.457(7)	1.4643(9)	1.454(3)
C(2)−C(3)	1.521(2)	1.5209(9)	1.5094(19)	1.522(6)	1.5121(12)	1.504(4)
C(3)−N(2)	1.279(2)	1.2744(9)	1.2805(18)	1.2742(19)	1.2809(11)	1.267(3)
N(2)−C(4)	1.406(2)	1.4070(9)	1.4073(18)	1.4106(17)	1.4058(10)	1.416(3)
C(4)−C(5)	1.377(2)	1.375(1)	1.3783(18)	1.3785(18)	1.3665(11)	1.366(3)
C(5)−O(1)	1.368(2)	1.3600(8)	1.3630(15)	1.3655(16)	1.3594(9)	1.362(3)
O(1)−C(2)−C(3)	108.02(11)	108.09(5)	110.24(11)	109.4(4)	110.14(7)	110.6(2)
O(1)−C(2)−C(6)	105.09(11)	104.38(5)	105.7(3)	112.1(3)	106.26(6)	109.6(2)
N(1)−C(2)−O(1)	112.15(11)	112.65(5)	111.6(3)	106.2(4)	110.01(6)	106.9(2)
N(1)−C(2)−C(3)	108.16(12)	107.82(5)	109.3(3)	109.3(3)	110.38(7)	110.4(2)
φ^f/Å	0.121	0.117[j]	0.113	0.135	0.094	0.064
χ^g/Å	0.605	0.572	0.558	−0.483	0.277	
Ψ^h/Å	0.255	0.263	0.319	0.285	0.298	
ω^i/deg	351.0	350.3	345.7	348.4	347.3	349.0

[a] See ref 76 for crystal data and refinement parameters. [b] Reference 46. [c] Reference 77. [d] Spirooxazine **3**-SO crystallized with two crystallographically independent molecules in the asymmetric unit, denoted here as (a) and (b). [e] Reference 78. [f] φ = rms deviation of the oxazine ring atoms from the plane of the oxazine ring. [g] χ = distance of C(2) from the plane of the arene ring systems. [h] Ψ = distance of N(1) from the C(1)−C(2)−C(9) mean plane. [i] ω = Σ[C(1)−N(1)−C(2), C(1)−N(1)−C(9), C(2)−N(1)−C(9)]. [j] Chamontin et al.[77] cite a value of 0.010 Å for φ, but from the available structural data we calculated a value of 0.117 Å.

(**16**-SO)[77] and spiro[indoline-naphthoxazine] (**17**-SO),[78] are summarized in Table 3. In the closed forms of the spiroxazines, the naphthoxazine moiety is held nearly orthogonal to the azaheterocyclic moiety. The oxazine ring is puckered, and its deviation from planarity can be parametrized by the root-mean-square (rms) deviation of the oxazine ring atoms from the oxazine ring mean plane (φ). The values of φ range from 0.064 Å for **17**-SO to 0.135 Å for **3**-SO(b). The oxazine ring puckering in spirooxazines is such that the ring is folded into an envelope conformation along the O(1)···C(3) axis, and the oxazine fragment either bends toward the N−Me group or away from it. The direction and extent of bending can be described geometrically by the distance of the C(2) atom from the mean plane of the arene ring system (χ), where a positive number indicates bending toward the N−Me group. Of the structures presented here, all have the oxazine fragment bent toward the N−Me group (χ = 0.605 to 0.277 Å), with the exception of one of the two distinct **3**-SO molecules, namely **3**-SO(b), in which the isoquinoline moiety bends away from the N−Me group (χ = −0.483 Å). Folding of the pyran ring in both directions has been reported in the literature for several closed-form spiropyran derivatives, including within the same crystal for crystallographically independent molecules. This geometric feature may therefore be largely influenced by packing effects.[42]

Correlations have been found between the long C_{spiro}−O bond lengths (1.45−1.50 Å) of spirooxazines [relative to the typical C−O bond length of an oxygen-containing six-membered heterocycle (1.41−1.43 Å)][79] and their degree of photocolorability.[42,68,80] The effect of aromatic ring structure on the C_{spiro}−O bond length of the oxazine can be seen across the series of compounds. The C_{spiro}−O bond of the azahomoadamantyl isoquinoline derivative **1**-SO [C(2)−O(1) = 1.490(2) Å] is greater by 0.013 Å than that of the azahomoadamantyl naphthalene derivative **16**-SO [C(2)−O(1) = 1.4767(7) Å]. In the indolyl series, a slight increase in the C_{spiro}−O bond length from 1.454(3) Å for the naphthalene derivative **17**-SO to 1.4585(16)/1.457(7) Å for the isoquinoline derivative **3**-SO (a/b) to 1.4643(9) Å for the phenanthroline derivative **4**-SO is observed. Additionally, the C_{spiro}−O bond lengths for the naphthalene and isoquinoline azahomoadamantyl derivatives are 0.02−0.03 Å longer than those for the analogous indolyl derivatives.

One of the parameters that has been used to describe the geometry of the indoline moiety, and which can be extended to the azahomoadamantyl moieties, is the planarity of the N(1)R_3 group, parametrized either by the distance of the N(1) atom from the R_3 plane (Ψ) or by the total sum of the three R−N(1)−R angles (ω) (Table 3). The values of Ψ range from 0.255 Å for **1** to 0.319 Å for **3**-SO(a), and the values of ω range from 345.7° for **3**-SO(a) to 351.0° for **1**-SO. The results suggest a greater degree of planarity about the amine moiety in the azahomoadamantyl derivatives relative to the indolyl derivatives. Typically, spirooxazines have N(1)−C(2) bond lengths which are shorter than those expected for a C−N bond in a five-membered heterocycle (1.47−1.48 Å).[43,79] This is the case in all of the spirooxazines discussed here, in which the N(1)−C(2) bond lengths range from 1.4311(8) Å for **16**-SO to 1.454(4) Å for **3**-SO(b).

X-ray Diffraction Analysis of the Photomerocyanine Forms. Dark purple single crystals of **1**-PMC were obtained upon continuous UV irradiation ($250 < \lambda < 400$ nm, 6 mW) of a dilute hexane solution of **1** for 1 h (see ref 81 for crystal data and refinement parameters). The photomerocyanine crystallized in the monoclinic $P2_1/c$ space group with four molecules in the unit cell (Figure 6). The molecules pack in head-to-tail dimeric units (as in H aggregation) with parallel isoquinoline groups and large intermolecular mean plane separations of 4.62 Å (Figure 6, bottom). These dimeric units assemble lengthwise to form a series of perpendicularly arranged chains running along the *c* axis. The chains are arranged such that additional close intermolecular N(1)···O(1) contacts of 3.39 Å occur between chains, slightly greater than the expected van der Waal's atom−atom contact of 3.2 Å.

Dark purple single crystals of **2**-PMC were obtained as two pseudopolymorphs—a crystalline lattice without solvent inclu-

(77) Chamontin, K.; Lokshin, V.; Guglielmetti, R.; Samat, A.; Pèpe, G. *Acta Crystallogr., Sect. C: Cryst. Struct. Commun.* **1998**, *54*, 670–672.
(78) Millini, R.; Del Piero, G.; Allegrini, P.; Crisci, L.; Malatesta, V. *Acta Crystallogr., Sect. C: Cryst. Struct. Commun.* **1991**, *47*, 2567–2569.
(79) Allen, F. H.; Kennard, O.; Watson, D. G.; Brammer, L.; Orpen, A. G.; Taylor, R. *J. Chem. Soc., Perkin Trans. 2* **1987**, (12), S1–S19.
(80) Millini, R.; Del Piero, G.; Allegrini, P.; Malatesta, V.; Castaldi, G. *Acta Crystallogr., Sect. C: Cryst. Struct. Commun.* **1993**, *49*, 1205–1207.

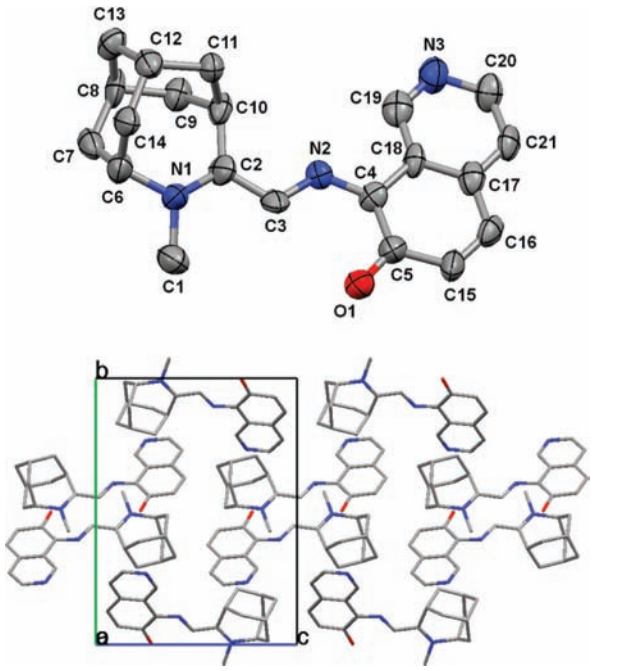

Figure 6. Molecular structure of **1**-PMC with thermal ellipsoids shown at the 50% probability level (top) and crystal packing viewed along the *a* axis (bottom).

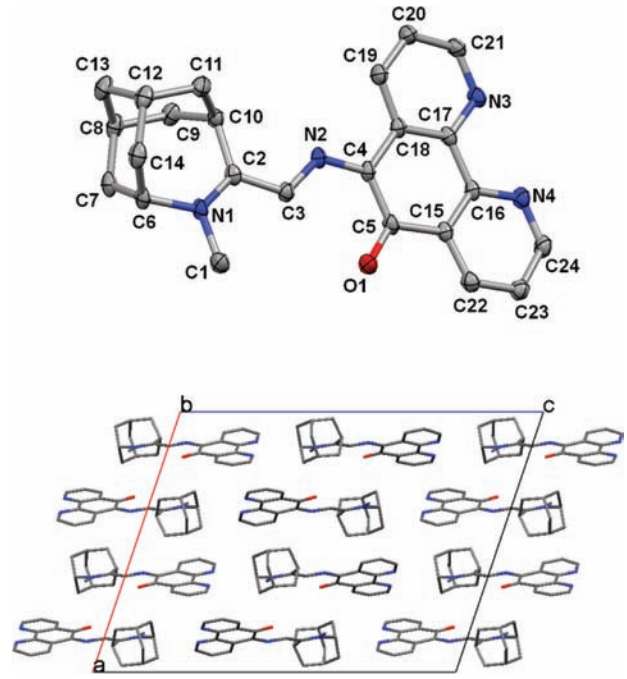

Figure 7. Molecular structure of **2**-PMC-I with thermal ellipsoids shown at the 50% probability level (top) and crystal packing viewed along the *b* axis (bottom).

sion (**2**-PMC-I) and a trihydrate of the PMC form (**2**-PMC-II)—from the slow evaporation of ethyl acetate (see ref 81 for crystal data and refinement parameters). The unsolvated pseudopolymorph of azahomoadamantyl phenanthroline photomerocyanine, **2**-PMC-I, crystallized in the monoclinic *C*2/*c* space group with eight molecules in the unit cell (Figure 7). The molecules pack as slipped head-to-tail dimeric units with large intermolecular mean plane separations of 4.64 Å (Figure 7, bottom). These dimeric units assemble into chains running along the *c* axis in which each dimeric unit is tilted with respect to the last. Intermolecular N(1)···O(1) contacts of 4.49 Å are observed between chains.

The solvate of azahomoadamantyl phenanthroline photomerocyanine, **2**-PMC-II, crystallized in the $P2_1/n$ space group with four molecules in the unit cell (Figure 8). The presence of solvent molecules in the lattice caused significant disorder, and the structure was solved as a trihydrate with three water molecules per photomerocyanine molecule (see Supporting Information). Although the quality of the data for this structure

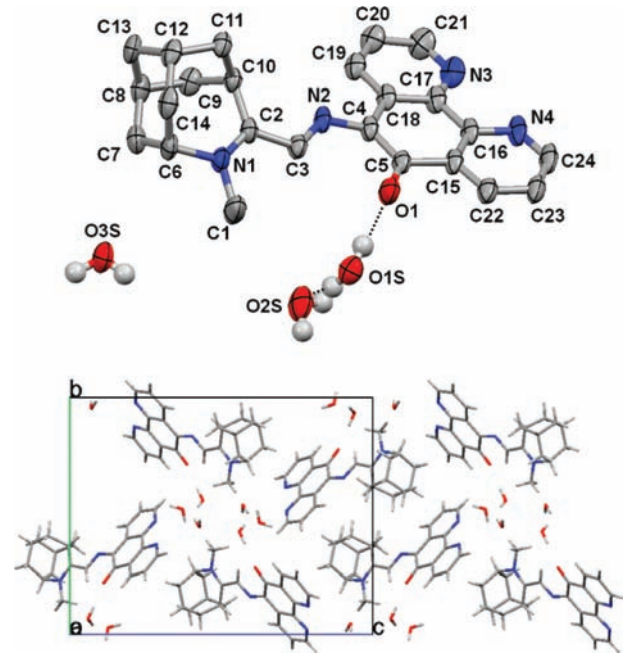

Figure 8. Molecular structure of **2**-PMC-II with thermal ellipsoids shown at the 50% probability level (top) and crystal packing viewed along the *a* axis (bottom).

was high [$R_{(int)}$ = 0.0661 on 4020 reflections], the solvent-induced disorder contributed to high *R* indices [R_1 = 0.0906, wR_2 = 0.2565]. The unit cell contains four molecules that are oriented about six water molecules to give a water cavity formed in the *b*/*c* plane. Strong hydrogen bonds exist between the heterocyclic ring oxygen, O(1), and closest H_2O molecule, O(1S), [H(1S)···O(1) = 1.880 Å] (Figure 8, bottom) with additional hydrogen bonding (H···O = 1.900 Å) between remaining water molecules. The water molecules form a hydrogen-bonded chain along the *a* axis, leading to a water

(81) **1-PMC.** Formula: $C_{21}H_{23}N_3O$. FW: 333.42 g mol^{-1}. Crystal system: monoclinic. Space group: $P2_1/c$. *a*: 9.2890(10) Å. *b*: 15.728(2) Å. *c*: 12.7750(9) Å. β: 111.391(5)°. *V*: 1737.8(3) Å^3. *Z*: 4. ρ_{calc}: 1.274 mg mm^{-3}. μ: 0.080 mm^{-1}. *T*: 130(2) K. ρ: 0.71073 Å. R_1: 0.0622. wR_2: 0.1604. $R_1 = \sum||F_o|-|F_c||/\sum|F_o|$; $wR_2 = [\sum w(F_o^2 - F_c^2)^2/\sum w(F_o^2)]^{1/2}$; $w = [\sigma^2(F_o^2) + (0.0000P)^2 + 0.0000P]^{-1}$ where $P = [F_o^2 + 2F_c^2]/3$). **2-PMC-I.** Formula: $C_{24}H_{24}N_4O$. FW: 384.47 g mol^{-1}. Crystal system: monoclinic. Space group: *C*2/*c*. *a*: 18.7530(18) Å. *b*: 8.7476(8) Å. *c*: 24.797(3) Å. β: 108.605(5)°. *V*: 3855.3(7) Å^3. *Z*: 8. ρ_{calc}: 1.325 mg mm^{-3}. μ: 0.083 mm^{-1}. *T*: 110(2) K. ρ: 0.71073 Å. R_1: 0.0469. wR_2: 0.1174. $R_1 = \sum||F_o| - |F_c||/\sum|F_o|$; $wR_2 = [\sum w(F_o^2 - F_c^2)^2/\sum w(F_o^2)]^{1/2}$; $w = [\sigma^2(F_o^2) + (0.0735P)^2 + 2.1923P]^{-1}$ where $P = [F_o^2 + 2F_c^2]/3$). **2-PMC-II.** Formula: $C_{24}H_{24}N_4O\cdot 3H_2O$. FW: 438.52 g mol^{-1}. Crystal system: monoclinic. Space group: $P2_1/n$ (an alternate setting of $P2_1/c$). *a*: 6.6536(12) Å. *b*: 16.165(3) Å. *c*: 20.809(4) Å. β: 93.277(2)°. *V*: 2234.4(7) Å^3. *Z*: 4. ρ_{calc}: 1.304 mg mm^{-3}. μ: 0.090 mm^{-1}. *T*: 193 K. ρ: 0.71073 Å. R_1: 0.0906. wR_2: 0.2565. $R_1 = \sum||F_o| - |F_c||/\sum|F_o|$; $wR_2 = [\sum w(F_o^2 - F_c^2)^2/\sum w(F_o^4)]^{1/2}$; $w = [\sigma^2(F_o^2) + (0.1002P)^2 + 4.1726P]^{-1}$ where $P = [\text{Max}(F_o^2, 0) + 2F_c^2]/3$).

Table 4. Selected Bond Lengths [Å] and Angles [deg] for **1**-PMC and **2**-PMC (I and II)[a]

	1-PMC	**2**-PMC-I	**2**-PMC-II
C(1)−N(1)	1.485(9)	1.478(5)	1.473(6)
N(1)−C(2)	1.337(9)	1.327(2)	1.313(5)
C(2)−C(3)	1.445(9)	1.427(2)	1.448(5)
C(3)−N(2)	1.319(8)	1.326(2)	1.315(5)
N(2)−C(4)	1.374(8)	1.346(2)	1.359(5)
C(4)−C(5)	1.447(11)	1.442(2)	1.423(6)
C(5)−O(1)	1.266(10)	1.249(2)	1.245(5)
N(1)−C(2)−C(3)−N(2) [α]	173.55	179.17	170.85
C(2)−C(3)−N(2)−C(4) [β]	175.43	−174.93	176.41
C(3)−N(2)−C(4)−C(5) [γ]	−4.99	1.45	−13.29

[a] See ref 81 for crystal data and refinement parameters.

channel as a result of cooperative hydrogen bonding (Supporting Information).

The experimental bond lengths and angles defining the central conjugated azomethine bridge are tabulated in Table 4 for **1**-PMC and **2**-PMC. Prediction of the theoretical limit for a pure canonical quinoidal form (Scheme 1, **A**) using average bond lengths[79] leads to a predicted geometry along the azomethine bridge with bond lengths of N(1)−C(2) = 1.355(14) Å, C(2)−C(3) = 1.360(20) Å, C(3)−N(2) = 1.376(11) Å, N(2)−C(4) = 1.279(8) Å, and C(4)−C(5) = 1.478(11). A similar prediction of the structure of the zwitterionic form (Scheme 1, **B**) leads to bond lengths of N(1)−C(2) = 1.316(9) Å, C(2)−C(3) = 1.460(15) Å, C(3)−N(2) = 1.279(8) Å, N(2)−C(4) = 1.376(11) Å, and C(4)−C(5) = 1.364(14) Å. For **1**-PMC, the three bonds that make up the azomethine bridge [C(2)−C(3), C(3)−N(2), and N(2)−C(4)] exhibit bond-length alternation with predominantly single-bond [1.445(9) Å], double-bond [1.319(8) Å], and single-bond [1.374(8) Å] character, respectively. The direction of bond-length alternation and absolute bond lengths are close to those expected for the zwitterionic form **B**. The C(5)−O(1) bond length [1.266(10) Å] falls between those expected for a quinoidal C═O bond [1.222(13) Å][79] and a zwitterionic phenoxyl C−O bond [1.362(15) Å],[79] although it is closer to that expected for a C═O quinoidal bond.

The availability of two pseudopolymorphs for **2**-PMC provides insight into the effects of chemical environment on the structure of the PMC form. Although the refined structure for **2**-PMC-II has a high degree of disorder and lower quality refinement parameters ($R_1 = 0.0906$, $wR_2 = 0.2565$) relative to **2**-PMC-I ($R_1 = 0.0469$, $wR_2 = 0.1174$), differences between several of the bond lengths for the two structures are equal to or greater than 2σ (Table 4, Supporting Information), which suggests that they are crystallographically significant. Notable differences are observed along the azomethine bridge. In **2**-PMC-I, the bond lengths along the bridge [C(2)−C(3) = 1.427(2) Å, C(3)−N(2) = 1.326(2) Å, and N(2)−C(4) = 1.346(2) Å] fall between those expected for a quinoidal form (**A**) and a zwitterionic form (**B**), though they lean closer to those expected for the zwitterionic form. In contrast, the corresponding bond lengths in **2**-PMC-II [C(2)−C(3) = 1.448(5) Å, C(3)−N(2) = 1.315(5) Å, and N(2)−C(4) = 1.359(5) Å] exhibit the same bond-length alternation pattern, but with a shifting of bond lengths toward those expected for the zwitterionic resonance form by 0.011−0.021 Å, which suggests that **2**-PMC-II has more zwitterionic character. Additionally, a decrease in length of the adjacent C(4)−C(5) bond by 0.019 Å is observed in **2**-PMC-II relative to **2**-PMC-I, as expected with a shift to a more zwitterionic structure. In both moleules, the C(5)−O(1) bond retains predominantly quinoidal character with a length of 1.249(2) Å in **2**-PMC-I and 1.245(5) Å in **2**-PMC-II.

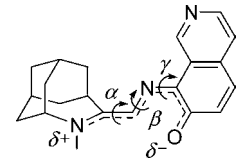

Figure 9. Torsional angles α, β, and γ about the azomethine bridge illustrated for **1**-PMC.

Table 5. Selected Bond Lengths [Å] Calculated at the DFT/B3LYP Level with the 6-31G(d,p) Basis Set for **1**-SO, **2**-SO, and **4**-SO

	1-SO			**4**-SO	
	calcd[a]	exptl[b]	2-SO	calcd	exptl
C(1)−N(1)	1.462	1.463(2)	1.462	1.453	1.4610(11)
N(1)−C(2)	1.429	1.431(2)	1.422	1.449	1.4454(11)
C(2)−O(1)	1.488	1.490(2)	1.495	1.467	1.4643(9)
C(2)−C(3)	1.527	1.521(2)	1.532	1.514	1.5121(12)
C(3)−N(2)	1.280	1.279(2)	1.278	1.282	1.2809(11)
N(2)−C(4)	1.401	1.406(2)	1.403	1.400	1.4058(10)
C(4)−C(5)	1.389	1.377(2)	1.375	1.373	1.3665(11)
C(5)−O(1)	1.357	1.368(2)	1.358	1.357	1.3594(9)

[a] Calculated with the 6-31G(d) basis set. [b] Reference 46.

The torsional angles α, β, and γ [α = N(1)−C(2)−C(3)−N(2), β = C(2)−C(3)−N(2)−C(4), and γ = C(3)−N(2)−C(4)−C(5); Figure 9] relevant to the cisoid or transoid character about the azomethine bridge are tabulated in Table 4. For each of the three PMC structures, these angles deviate slightly from those expected for a fully planar *trans-trans-cis* (or "TTC") configuration (180°, 180°, and 0°), which suggests that this isomer is the most stable in the crystalline state, consistent with results observed for similar molecules.[42,44,45] The total deviation from planarity, as determined by the sum of the deviation from 0° or 180° for each of the three angles, differs considerably for the three structures, where **1**-PMC, **2**-PMC-I, and **2**-PMC-II have total deviations of 16.01°, 7.35°, and 26.03°, respectively.

Computational Results. Geometry optimization calculations for the SO and PMC forms of **1**, **2**, and **4** were performed at the DFT/B3LYP level with the 6-31G(d,p) basis set using the Gaussian 03 suite of software. Selected parameters are summarized in Tables 5 and 6. Additional calculations with the 6-31+G(d,p), 6-311G(d,p), and 6-311+G(d,p) basis sets were performed on **2**-PMC (Supporting Information); however, larger basis sets did not significantly affect the optimized geometries (variations in bond lengths were ≤0.005 Å), which is consistent with previous computational studies.[82,83] For the PMC forms of the phenanthroline spirooxazine derivatives, **2**-PMC and **4**-PMC, geometry optimizations were also performed in toluene ($\varepsilon = 2.379$), DMSO ($\varepsilon = 46.7$), and water ($\varepsilon = 78.39$) using the Onsager model, although the results obtained in water were nearly identical to those obtained in DMSO, and therefore only the results obtained for DMSO are tabulated here.

Comparison of the computational geometries for the closed forms of the azahomoadamantyl derivatives allows reasonable prediction regarding their molecular structure, as is evident by the good correlations between calculated and experimental geometries. Optimized geometries (Table 5) of the isoquinoline

(82) Sheng, Y. H.; Leszczynski, J.; Garcia, A. A.; Rosario, R.; Gust, D.; Springer, J. *J. Phys. Chem. B* **2004**, *108* (41), 16233–16243.
(83) Maurel, F.; Aubard, J.; Rajzmann, M.; Guglielmetti, R.; Samat, A. *J. Chem. Soc., Perkin Trans. 2* **2002**, (7), 1307–1315.

Table 6. Selected Geometric Parameters (Bond Lengths [Å] and Angles [deg]) and Dipole Moments [D] Calculated at the DFT/B3LYP Level with the 6-31G(d,p) Basis Set for **1**-PMC, **2**-PMC, and **4**-PMC with and without Solvation Using the Onsager Model

	1-PMC[a]		**2**-PMC				**4**-PMC		
	no medium	exptl	no medium	toluene	DMSO	exptl[b]	no medium	toluene	DMSO
ε	0		0	2.379	46.7		0	2.379	46.7
C(1)−N(1)	1.468	1.485(9)	1.467	1.469	1.472	1.478(5)	1.454	1.455	1.460
N(1)−C(2)	1.357	1.337(9)	1.358	1.353	1.343	1.327(2)	1.369	1.363	1.348
C(2)−C(3)	1.405	1.445(9)	1.403	1.409	1.422	1.427(2)	1.385	1.391	1.409
C(3)−N(2)	1.344	1.319(8)	1.346	1.341	1.331	1.326(2)	1.351	1.345	1.331
N(2)−C(4)	1.325	1.374(8)	1.322	1.326	1.335	1.346(2)	1.320	1.324	1.339
C(4)−C(5)	1.488	1.447(11)	1.480	1.474	1.464	1.442(2)	1.484	1.478	1.462
C(5)−O(1)	1.244	1.266(10)	1.241	1.242	1.244	1.249(2)	1.239	1.240	1.245
α	−179.99	173.55	−179.20	−179.16	−179.04	179.17	−179.97	−179.98	−179.98
β	180	175.43	−179.19	−179.30	−179.53	−174.93	179.99	179.99	179.99
γ	−0.01	−4.99	0.18	0.14	0	−1.45	−0.01	0.01	−0.00
dipole (*x*)	5.8789		9.0405	11.5458	16.1694		7.00	10.0077	18.2626
dipole (*y*)	1.09		1.68	1.98	2.44		1.43	1.66	2.01
dipole (*z*)	0.0005		0.0062	0.019	0.041		0.0008	0.0009	0.0009
total dipole	5.98		9.20	11.71	16.35		7.15	10.14	18.37

[a] Optimized using initial coordinates from the X-ray structure geometry. [b] The experimental geometry for **2**-PMC-I was arbitrarily chosen.

and phenanthroline derivatives, **1**-SO and **2**-SO, reveal subtle differences in geometry. The most significant effects predicted upon heterocyclic ring expansion are an increase in the C(2)−O(1) bond length by 0.007 Å and a decrease in the N(1)−C(2) bond length by 0.007 Å, consistent with the observed increase in photocolorability for **2**-SO. A predicted decrease in the C(4)−C(5) bond length by 0.014 Å is consistent with greater double-bond character of the 5,6-positions of the phenanthroline ring. More significant differences in bond lengths are predicted for the oxazine and amine moiety of the azahomoadamantyl and indolyl phenanthroline derivatives **2**-SO and **4**-SO, as expected. Substitution of azahomoadamantyl for indolyl leads to a predicted increase in the N(1)−C(2) bond length by 0.027 Å and decrease in the C(2)−O(1) bond length by 0.028 Å, consistent with the lower photocolorability of **4**-SO.

DFT predicts very similar structures for **1**-PMC and **2**-PMC with regard to the bond lengths and angles in the azomethine bridge (Table 6). The optimized bond lengths in the bridge [C(2)−C(3), C(3)−N(2), and N(2)−C(4)] for both molecules lie nearly exactly between those expected for resonance forms **A** and **B**, which would indicate approximately equal contributions from the two forms. This result is consistent with previous calculations on spirooxazines.[83] The optimized bond lengths for the C(1)−N(1), N(1)−C(2), and C(4)−C(5) bonds are within 0.005 Å of those expected for the quinoidal resonance form **A**. The predicted C(5)−O(1) bond lengths of 1.244 Å in **1**-PMC and 1.241 Å in **2**-PMC are only slightly longer than a quinoidal C═O double bond (1.221 Å)[79] and significantly shorter than a C−O single bond (1.362 Å).[79] For the indoline phenanthroline derivative, **4**-PMC, the C(1)−N(1) and N(1)−C(2) bond lengths are predicted to be shorter and longer, respectively, than those expected for resonance form **A**. Of the remaining bond lengths, all are within 0.005 Å of those obtained for **2**-PMC except for the C(2)−C(3) bond length which is 0.018 Å shorter. This result indicates that the DFT-optimized geometries are quite similar for both the indolyl and azahomoadamantyl derivatives as regards the structure of the central bridge. However, the deviations observed, particularly for the C(2)−C(3) bond, suggest that the structure for **4**-PMC has a slightly greater contribution from the quinoidal resonance form **A**. For all of the molecules, the optimized dihedral angles α, β, and γ are very close to 180°, 180°, and 0°, respectively, with the total deviation from planarity for the three angles not exceeding 2°. DFT calculations thus predict a highly planar structure relative to the experimental structures, consistent with the tendency of DFT to favor delocalized geometries.

Optimization of the geometries in solvents with varying dielectric constants using the Onsager model has a significant effect on the resulting structure for **2**-PMC and **4**-PMC. In both derivatives, the N(1)−C(2), C(2)−C(3), C(3)−N(2), N(2)−C(4), and C(4)−C(5) bond lengths deviate by 0.002−0.006 Å in toluene or 0.010−0.020 Å in DMSO relative to those predicted in the gas phase, in each case becoming closer to those expected for the zwitterionic resonance form **A**. The calculated C(5)−O(1) bond length, however, was found to be only 0.001 and 0.003−0.006 Å longer in toluene and DMSO, respectively.

The calculations predict large dipole moments along the long axis of the molecule for all of the PMC forms. The total dipole moments were found to be 5.98, 9.20, and 7.15 D for **1**-PMC, **2**-PMC, and **4**-PMC, respectively, with the major contribution being along the *x* axis (long axis). For both **2**-PMC and **4**-PMC, the dipole moment increases significantly for calculations performed in higher dielectric media: for **2**-PMC, the total dipole moment increased to 11.71 and 16.35 D in toluene and DMSO, respectively, and for **4**-PMC, it similarly increased to 10.14 and 18.37 D in toluene and DMSO, respectively. This suggests an increase in charge-separated state with increasing polarity of the media.

Discussion

Vibrational Structure and Solvatochromism of the Electronic Absorption Spectra of the Indolyl and Azahomoadamantyl Photomerocyanines. The molecular structure of merocyanines can be probed indirectly by electronic absorption spectroscopy as a function of solvent polarity by analyzing either (a) the relative geometries of the ground and excited states inferred from the relative intensities of the vibrational bands of the $\pi-\pi^*$ electronic transition[84,85] or (b) the solvent-induced stabilization of the ground and excited states inferred from the shift in energy of the absorption band, i.e., its solvatochromism.[86] The inferred structural changes may be interpreted in the context of the relative contributions of the canonical quinoidal (**A**) and

(84) Hiramatsu, T.; Yoshida, H.; Sato, N. *J. Phys. Chem. A* **2009**, *113* (32), 9174–9179.
(85) Mustroph, H.; Reiner, K.; Mistol, J.; Ernst, S.; Keil, D.; Hennig, L. *ChemPhysChem* **2009**, *10* (5), 835–840.
(86) Buncel, E.; Rajagopal, S. *Acc. Chem. Res.* **1990**, *23* (7), 226–231.

zwitterionic (**B**) resonance forms to the ground-state molecular structure (Scheme 1).[84]

Vibronic progressions are commonly observed in the $\pi-\pi^*$ charge transfer bands of merocyanines, where, in addition to a $\nu = 0 \rightarrow \nu' = 0$ transition, higher energy ($\nu = 0 \rightarrow \nu' = 1$, $\nu = 0 \rightarrow \nu' = 2$, etc.) transitions are evident as coarse band structure.[85,87,88] The major vibrational mode associated with the electronic transition in typical merocyanines is a C═C symmetric stretch, in which the C═C bonds are expected to lengthen in the excited state.[85] The spirooxazine-based photomerocyanines display an analogous vibronic progression in their electronic absorption spectra,[89,90] presumably associated with similar symmetric modes involving the conjugated bridge. For a fully delocalized conjugated structure resulting from equal contributions of resonance forms **A** and **B**, small changes in geometry would be expected between ground and excited states, and the Franck−Condon overlap model dictates that the $\nu = 0 \rightarrow \nu' = 0$ transition should dominate the charge transfer band. For predominantly quinoidal (**A**) or zwitterionic (**B**) structures with localized bond alternation throughout the conjugated bridge, more significant differences in geometry are expected between the ground and excited states, and transitions to higher ν' vibrational states should intensify relative to the $\nu = 0 \rightarrow \nu' = 0$ transition.

As regards the solvatochromism of photomerocyanines, three scenarios can be identified based on the solvatochromic behavior of typical merocyanine dyes:[91] (1) for a quinoidal (**A**) ground-state structure, a more dipolar excited state should exhibit greater stabilization with increasing solvent polarity, and a bathochromic shift should result (i.e., positive solvatochromism); (2) for a zwitterionic (**B**) ground-state structure, a more dipolar ground state should exhibit greater stabilization with increasing solvent polarity, and a hypsochromic shift should be observed (i.e., negative solvatochromism); and (3) for a hybrid structure possessing equal contributions from the resonance forms **A** and **B**, the moderately dipolar ground and excited states should be equally stabilized with increasing solvent polarity, and no significant solvatochromic shift should result.[86]

The solvatochromic behavior of merocyanines has been heavily investigated and remains controversial.[92] Key points of contention have been the relationship of solvatochromic behavior to molecular structure, as well as the origin of the experimentally observed phenomenon of "inverted solvatochromism", where a switch in overall solvatochromic behavior is observed with a change in solvent polarity.[73,86,93] Theoretical studies have correlated experimentally observed solvatochromic effects with molecular structure; calculations at various levels of theory predict significant changes in dipole moment and molecular structure upon increasing the dielectric constant of the surrounding medium, which indicate a clear transition from greater quinoidal character in the gas phase or nonpolar solvents to greater charge-separated zwitterionic character in polar solvents.[91,93–97] Recent electro-optical absorption studies have confirmed that such structural changes do indeed result from polarization effects in polar solvents.[88] Several authors have proposed alternative explanations for the experimentally observed solvatochromic behaviors of merocyanines including interactions between permanent solute dipoles and induced solvent dipoles,[84] as well as solvent-induced changes in molecular aggregation,[98] vibrational structure,[87] or distribution of *cis*/*trans* isomers in solution.[99] It has been suggested that analysis of the vibronic intensity profile is a more reliable method than analysis of the solvatochromism of the absorption band toward predicting molecular structure.[84] Indeed, interpretation of solvatochromic effects may be case-dependent, and one must proceed with caution, particularly when interpreting solvatochromic trends in electronic absorption spectra exhibiting coarse structural features where effects associated with these features can be convoluted with solvatochromic effects.

In order to thoroughly interpret the solvatochromism of the spirooxazines under investigation, we examined both the vibrational structure and λ_{max} values of their PMC $\pi-\pi^*$ absorption bands in a large selection of solvents. We observed different vibrational intensity profiles and solvatochromic behavior for the azahomoadamantyl and indolyl PMCs, but in both types of derivatives a qualitative reversal in behavior was observed in solvents with moderate-polarity values of $E_T^N \approx 0.3-0.6$.

The Lorentzian deconvoluted $\nu(1)$, $\nu(2)$, and $\nu(3)$ bands of the PMC $\pi-\pi^*$ band can be assigned to $\nu = 0 \rightarrow \nu' = 0$, $\nu = 0 \rightarrow \nu' = 1$, and $\nu = 0 \rightarrow \nu' = 2$ vibrational transitions, respectively, in accordance with the spectroscopic features of typical merocyanines. For the azahomoadamantyl derivative, **2**-PMC, an increase in intensity of $\nu(1)$ with a corresponding decrease in intensity of $\nu(2)$ and $\nu(3)$ is observed in lower polarity solvents, followed by a decrease in intensity of $\nu(1)$ with a corresponding increase in intensity of $\nu(2)$ and $\nu(3)$ in higher polarity solvents [Figure 3(a)], where the change in behavior is observed at $E_T^N \approx 0.5-0.6$. This is consistent with the ground- and excited-state molecular structures being most similar in moderate polarity solvents when the $\nu = 0 \rightarrow \nu' = 0$ transition dominates; a more quinoidal structure is expected in lower polarity solvents, and a more zwitterionic structure is expected in higher polarity solvents. In contrast, for the indolyl derivative **4**-PMC, an increase in intensity of $\nu(1)$ with a corresponding decrease in intensity of $\nu(2)$ and $\nu(3)$ is likewise observed in lower polarity solvents, but this is followed by a leveling off of the intensities of the three bands, with a possible reversal in behavior observed at $E_T^N \approx 0.8$ [Figure 3(b)]. This behavior is consistent with the existence of a quinoidal structure in low polarity solvents, and a hybrid **A**/**B** structure in moderate- to high-polarity solvents.

As regards solvatochromic behavior, the azahomoadamantyl derivatives, **1**-PMC and **2**-PMC, exhibit a change from weakly

(87) Catalán, J.; Mena, E.; Meutermans, W.; Elguero, J. *J. Phys. Chem.* **1992**, *96* (9), 3615–3621.
(88) Würthner, F.; Archetti, G.; Schmidt, R.; Kuball, H.-G. *Angew. Chem., Int. Ed.* **2008**, *47* (24), 4529–4532.
(89) Pottier, E.; Dubest, R.; Guglielmetti, R.; Tardieu, P.; Kellmann, A.; Tfibel, F.; Levoir, P.; Aubard, J. *Helv. Chim. Acta* **1990**, *73* (2), 303–315.
(90) Ernsting, N. P.; Arthen-Engeland, T. *J. Phys. Chem.* **1991**, *95* (14), 5502–5509.
(91) Botrel, A.; Lebeuze, A.; Jacques, P.; Strub, H. *J. Chem. Soc., Faraday Trans. 2* **1984**, *80*, 1235–1252.
(92) Mishra, A.; Behera, R. K.; Behera, P. K.; Mishra, B. K.; Behera, G. B. *Chem. Rev.* **2000**, *100* (6), 1973–2011.
(93) da Silva, L.; Machado, C.; Rezende, M. C. *J. Chem. Soc., Perkin Trans. 2* **1995**, (3), 483–488.
(94) Benson, H. G.; Murrell, J. N. *J. Chem. Soc., Faraday Trans. 2* **1972**, *68* (590), 137–143.
(95) Albert, I. D. L.; Marks, T. J.; Ratner, M. A. *J. Phys. Chem.* **1996**, *100* (23), 9714–9725.
(96) Morley, J. O.; Morley, R. M.; Docherty, R.; Charlton, M. H. *J. Am. Chem. Soc.* **1997**, *119* (42), 10192–10202.
(97) Baraldi, I.; Momicchioli, F.; Ponterini, G.; Vanossi, D. *Chem. Phys.* **1998**, *238* (3), 353–364.
(98) Niedbalska, M.; Gruda, I. *Can. J. Chem.* **1990**, *68* (5), 691–695.
(99) Tsukada, M.; Mineo, Y.; Itoh, K. *J. Phys. Chem.* **1989**, *93* (24), 7989–7992.

positive to strongly negative solvatochromism with increasing solvent polarity (Figure 4), which suggests that their ground-state structure progresses from quinoidal to zwitterionic in character. The negative solvatochromism of **1**-PMC is more pronounced than that of **2**-PMC, which suggests that **1**-PMC has more zwitterionic character. In contrast, the indolyl phenanthroline derivative, **4**-PMC, exhibits a change from relatively strong positive solvatochromism in low-polarity solvents to little or no solvatochromism in high-polarity solvents (Figure 4). This behavior suggests that the ground-state structure of **4**-PMC progresses from predominantly quinoidal in character to a hybrid **A**/**B** form with approximately equal contributions from the quinoidal and zwitterionic resonance structures with increasing solvent polarity. The positive solvatochromism observed for **4**-PMC in solvents with low to moderate E_T^N values is consistent with the observations previously reported by Pozzo et al,[31] although the authors did not highlight the absence of a solvatochromic shift at higher E_T^N values. For both **2**-PMC and **4**-PMC, the solvatochromism of the experimental PMC $\pi-\pi^*$ absorption band mirrors that of both the deconvoluted $\nu(1)$ and $\nu(2)$ bands; however, the deconvoluted $\nu(3)$ band exhibits negative solvatochromism over the full range of solvent polarities. This observation can be rationalized by the possibility of different solvatochromic responses for different vibrational bands, as has been experimentally demonstrated by Würthner et al., who have associated the effect with a change in molecular dipole of a given vibrational level in the excited state.[88] However, if this interpretation is correct, it begs the question of how the behavior of each vibrational band ultimately corresponds to the molecular structure of the merocyanine.

It is of interest that the qualitative reversal in behavior of the vibrational band intensity profile and solvatochromism as a function of solvent occurs at different solvent polarities, where the former is observed at slightly higher polarities. This observation is consistent with studies by Hiramatsu et al., who observe a similar effect and posit that the reversal of the vibrational band intensity profile behavior may be a more accurate indicator of the polarity at which the limiting structure possesses equal contributions of quinoidal and zwitterionic resonance character.[84] However, in their case, negative solvatochromism was not observed even in high polarity solvents as it was for the molecules described here, and our data may highlight the fact that molecular structure may still be inferred from solvatochromic behavior, with the knowledge that the limiting **A**/**B** form exists at slightly higher polarities than predicted by the solvatochromic reversal. This is supported by theoretical work by Botrel et al. who show that the limiting **A**/**B** form exists at slightly higher polarities than indicated by the solvatochromic data.[91]

It is unlikely that aggregation effects play a major role in the observed spectral shifts of **1**-PMC, **2**-PMC, and **4**-PMC as their $\pi-\pi^*$ transitions obey the Beer−Lambert law in both nonpolar and polar solvents, and no change in the appearance of their absorption bands is observed over a wide concentration range (Supporting Information). The occurrence of solute−solvent hydrogen bonding interactions in the azahomoadamantyl derivatives **1**-PMC and **2**-PMC in strong hydrogen-bond donating solvents is possible. We did not attempt to quantify the contributions of specific and nonspecific interactions to PMC solvation, though we expect that both polarization and H-bonding effects play comparable solvating roles in the high-E_T^N-value solvents, as has been found for similar systems.[70,73,96,100] Because there is no obvious steric reason for which the indolyl derivatives would not exhibit the same H-bonding effects as the azahomoadamantyl derivatives, this may suggest that solvation through H-bonding serves to stabilize the charge-separated character of molecules which have an intrinsically more stable zwitterionic structure rather than inducing a more zwitterionic structure through H-bonding interactions alone.

In summary, the degree of quinoidal or zwitterionic character of the ground-state PMC species in solution was found to dominate the observed solvatochromic behavior for the investigated spiroooxazines. The azahomoadamantyl derivatives clearly exhibit a reversal of the vibrational band intensity profile and a transition to negative solvatochromism in high polarity solvents that are absent in the analogous indolyl derivative. This suggests that the two families of spirooxazines possess fundamentally different ground-state molecular structures in which the degree of quinoidal or zwitterionic character in a given medium differs with increasing polarity of the solvent. The bicyclic derivatives progress from slightly quinoidal to zwitterionic in character, while the indolyl derivatives progress from quinoidal in character to a hybrid **A**/**B** form with increasing polarity. The overall possible range of quinoidal-to-zwitterionic character accessible by changing the solvent polarity is unique in the two classes, in which the bicyclic derivatives access a greater range of structures.

Analysis of Solution-State Structures by ^{1}H and ^{13}C NMR. ^{1}H and ^{13}C NMR studies were performed on **2** and **4** to obtain additional spectroscopic evidence for the molecular structures of the PMC forms with regard to both (a) the relative changes in PMC structure as a function of solvent polarity and (b) the absolute structures of **2**-PMC and **4**-PMC, whether they be more quinoidal (**A**) or zwitterionic (**B**) in character. To address (a), spectra of the spirooxazines were obtained in a range of solvents (Supporting Information). Solvent-dependent NMR studies on **4** have been previously reported by Pozzo et al.,[31] although in this study the authors used a more limited series of solvents. Limited success has been achieved in unambiguously correlating ^{1}H or ^{13}C NMR shifts to solvent-induced structural changes of merocyanines,[31,91,96] although good correlations between chemical shifts or J_{HH} coupling constants for merocyanines with extended polymethine chains have been reported.[85,101] To address (b), experimental NMR shifts were compared to theoretical shifts of model **A** and **B** forms.

As regards solvent polarity effects, a significant downfield shift in the *N*-methyl H-1 resonance of ∼1 ppm is observed when going from aromatic hydrocarbon solvents ($E_T^N \approx 0.1$) to higher polarity solvents ($E_T^N \approx 0.2-0.8$) for both **2**-PMC and **4**-PMC (Table 2). This may indicate a change in molecular structure upon going from very low to moderate/high polarity solvents, or could be explained by specific solvation effects (or lack thereof) in aromatic hydrocarbons. As regards absolute structures, comparison of the experimental and calculated H-3 shifts for **2**-PMC suggests that its structure can be approximated by nearly equal contributions of resonance forms **A** and **B**. Comparison of the experimental and calculated H-3 shifts for **4**-PMC, in contrast, suggests that its structure is closer to that of the quinoidal form **A**. Comparison of the experimental and calculated shifts for C-3 and C-5 predicts that the structures for

(100) Abdel-Halim, S. T. *J. Chem. Soc., Faraday Trans.* **1993**, *89* (1), 55–57.
(101) Kulinich, A. V.; Derevyanko, N. A.; Ishchenko, A. A. *J. Photochem. Photobiol., A* **2007**, *188* (2−3), 207–217.

2-PMC and **4**-PMC fall between those of resonance forms **A** and **B**, with more zwitterionic character overall and more zwitterionic character for **2**-PMC relative to **4**-PMC. The C-2 shifts predict significant zwitterionic character for both molecules. In summary, the NMR results do not emphatically support the change in molecular structure with solvent polarity suggested by the solvatochromism studies; however, the results do provide some evidence that the absolute structure of **2**-PMC is more zwitterionic than that of **4**-PMC, as inferred from the solvatochromism results, and that subtle shifts from quinoidal to more zwitterionic occur in the PMC forms in solution. The discrepancies between the solvatochromism and NMR shift results may be attributed to strong specific solvation effects that are expected to contribute significantly to NMR chemical shifts and to changes in molecular geometry. In general, deconvolution of the two effects is difficult for structures in which several geometries with similar energies can exist in solution.

Structures of the Closed Forms. The most important structural parameter in spirooxazines is undoubtedly their long $C_{spiro}-O$ bond length, a feature which is intimately related to their photochromic properties and typically associated with ease of bond cleavage.[34] The long $C_{spiro}-O$ bond length in the azahomoadamantyl isoquinoline derivative **1**-SO [1.490(2) Å] is consistent with that observed in a previously characterized bicyclic derivative,[102] and is on the order of the $C_{spiro}-O$ bond lengths found in nitro-[42] and pyridinium-substituted[103] indolyl spiropyrans (1.48−1.50 Å). The $C_{spiro}-O$ bond lengths in the indolyl isoquinoline and phenanthroline derivatives **3**-SO and **4**-SO (∼1.46 Å) are crystallographically equivalent to those found in previously characterized indolyl spirooxazine derivatives containing heterocyclic aromatics.[104−106]

The unusually long $C_{spiro}-O$ bond length in spirooxazines can be explained by specific orbital interactions facilitated by the hybridization and geometry about the spiro carbon. The $N-C_{spiro}$ and $C_{spiro}-O$ bonds are in the appropriate relative orientations to interact via the anomeric effect, where $n(N)-\sigma^*(C_{spiro}-O)$ donation is expected to lead to a decrease in the $N-C_{spiro}$ bond length and a corresponding increase in the $C_{spiro}-O$ bond length. An $n(O)-\pi^*(N-C_{spiro})$ interaction is also expected to be in effect—albeit to a lesser extent—and would have the opposite effect on the $N-C_{spiro}$ and $C_{spiro}-O$ bond lengths.[42,107] The increase in the $C_{spiro}-O$ bond length by 0.02−0.03 Å for the azahomoadamantyl isoquinoline (**1**-SO) and naphthalene (**16**-SO) derivatives relative to the respective indolyl derivatives (**3**-SO and **17**-SO) can be rationalized by a greater $n(N)-\sigma^*(C_{spiro}-O)$ interaction in the azahomoadamantyl compounds. The nitrogen lone pair is expected to be more available in the saturated bicyclic derivatives than in the conjugated indolyl derivatives. A stronger $n(N)-\sigma^*(C_{spiro}-O)$ interaction in the azahomoadamantyl derivatives is also corroborated by the relatively short $N-C_{spiro}$ bond lengths in **1**-SO [1.431(2) Å] and **16**-SO [1.4311(8) Å] relative to those in **3**-SO [1.439(7) Å for (a) and 1.454(4) Å for (b)] and **17**-SO [1.436(3) Å] [where an average $C(sp^3)$-$N(sp^3)$ bond length is 1.47−1.48 Å].[79] The long $C_{spiro}-O$ bond lengths and correspondingly short $N-C_{spiro}$ bond lengths in the azahomoadamantyl derivatives relative to the indolyl derivatives are consistent with the greater photocolorability observed for this family of spirooxazines.[46]

The availability of the N lone pair has been correlated with the degree of planarity of the NR_3 group (as parametrized here by Ψ and ω) for various indolyl derivatives.[107,108] In the azahomoadamantyl derivatives, however, the NR_3 group is actually closer to planarity than in any of the indolyl derivatives (Table 3). While there is little structural characterization for the 4-azahomoadamantane skeleton (4-azatricyclo[4.3.1.$1^{3,8}$]-undecane) beyond that published for the 4-azahomoadamantane-naphthalene spirooxazine discussed in this work,[77] it is clear from numerous reactivity studies of the 4-azahomoadamantane skeleton that 4-azatricyclo[4.3.1.$1^{3,8}$]undec-4-enes are in fact very stable.[109] This suggests that formation of an sp^2-hybridized nitrogen at the 4-position is thermodynamically favorable, distinct from formation of an anti-Bredt bridgehead imine, which in most bicyclics and tricyclics has not been isolated due to instability associated with Baeyer strain. In addition, crystal structure analysis of the corresponding lactone reveals a highly planar nitrogen, consistent with the observed planarity in the present work.

Correlations between the degree of oxazine ring puckering and photochromic parameters have been proposed. Explicitly, a higher degree of ring puckering has been correlated with higher photocolorabilities.[102,105] However, this has not always been found to be the case.[77] No strong correlation between ring puckering and photochromic parameters is apparent for the derivatives investigated here. It has alternatively been suggested that the conformation of the oxazine ring is determined by molecular sterics and crystal packing rather than electronic effects,[42] which would make correlation of this crystalline state structural feature with solution-state photochromic parameters challenging. The data presented here may corroborate the latter conclusion when one considers the relatively large difference in deviation from planarity of the oxazine ring (φ) found between the two crystallographically independent molecules in **3**-SO [0.113 Å for (a) and 0.135 Å for (b)].

Structures of the Photomerocyanine Forms and Effect of the Crystalline Environment. The molecular structures for **1**-PMC and **2**-PMC-II exhibit significant contributions from the zwitterionic resonance form **B**, as evidenced by a comparison of the experimental bond lengths with those expected for the canonical resonance forms **A** and **B** (Scheme 1). The nature of the zwitterionic bond-length alternation observed is consistent with that found in nitro-substituted indolyl spiropyrans.[42] The short C(5)−O(1) bond length and the relatively long C(4)−C(5) bond length observed in the experimentally characterized photomerocyanines (**1**-PMC, **2**-PMC-I, and **2**-PMC-II) suggest that these molecules possess contributions from the zwitterionic resonance form **C** in addition to **B**, in which a portion of the negative charge on the oxygen atom is delocalized onto the conjugated bridge and the C−O bond takes on greater quinoidal character (Scheme 5). This delocalization pattern is consistent

(102) Pèpe, G.; Laréginie, P.; Samat, A.; Zaballos, E. *Acta Crystallogr., Sect. C: Cryst. Struct. Commun.* **1995**, *51*, 1617–1619.
(103) Aldoshin, S. M.; Nikonova, L. A.; Smirnov, V. A.; Shilov, G. V.; Nagaeva, N. K. *Russ. Chem. Bull.* **2005**, *54* (9), 2113–2118.
(104) Osano, Y. T.; Mitsuhashi, K.; Maeda, S.; Matsuzaki, T. *Acta Crystallogr., Sect. C: Cryst. Struct. Commun.* **1991**, *47*, 2137–2141.
(105) Reboul, J.-P.; Samat, A.; Laréginie, P.; Lokshin, V.; Guglielmetti, R.; Pèpe, G. *Acta Crystallogr., Sect. C: Cryst. Struct. Commun.* **1995**, *51*, 1614–1617.
(106) Clegg, W.; Norman, N. C.; Flood, T.; Sallans, L.; Kwak, W. S.; Kwiatkowski, P. L.; Lasch, J. G. *Acta Crystallogr., Sect. C: Cryst. Struct. Commun.* **1991**, *47*, 817–824.
(107) Aldoshin, S. M.; Chuev, I. I.; Filipenko, O. S.; Utenyshev, A. N.; Lokshin, V.; Larégenie, P.; Samat, A.; Guglielmetti, R. *Russ. Chem. Bull.* **1998**, *47* (6), 1089–1097.
(108) Anisimov, V. M.; Aldoshin, S. M. *THEOCHEM* **1997**, *419*, 77–84.
(109) Averina, N. V.; Borisova, G. S.; Zefirov, N. S. *Russ. J. Org. Chem.* **2001**, *37* (7), 901–934.

Scheme 5. Resonance Forms of **1**-PMC

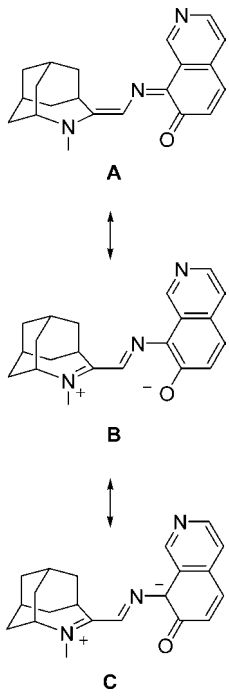

with the behavior observed in many of the structurally characterized zwitterionic photomerocyanines[38,42] as well as theoretical predictions of the electrostatic charge distributions[39] for related classes of photochromic molecules.

Comparison of the two pseudopolymorphs of **2**-PMC suggests that **2**-PMC-I has a greater contribution from the quinoidal resonance form **A** than does **2**-PMC-II, though both structures have more zwitterionic than quinoidal character in general. The differences between the pseudopolymorphs can be rationalized by a combination of molecular structure and crystal packing effects. There is a correlation between the degree of twisting about the three partial double bonds of the azomethine bridge and the degree of charge separation in the crystalline-state PMC structures: **2**-PMC-II displays a greater deviation from planarity and a correspondingly greater degree of zwitterionic-like bond-length alternation than does **2**-PMC-I. Whether this twisting is sterically or electronically imposed is not clear, although the existence of hydrogen bonding to water solvate molecules in **2**-PMC-II is expected to have a significant effect on the electronic structure of the PMC form through stabilization of the partial negative charge on the oxygen atom.

As regards possible electronic effects, each photomerocyanine has a large dipole moment directed along the long axis of the molecule, and the crystalline lattice itself can effectively act as a strong dielectric medium. This idea is corroborated by the fact that the solvatochromic behavior of **2**-PMC suggests that the photomerocyanine is slightly quinoidal in nonpolar solvents, while its crystal structures provide evidence for significant zwitterionic character. The molecular structure of the PMC form in the crystalline state may therefore be more similar to that expected in polar solvents than in nonpolar ones. The orientation of molecules in the highly ordered and unsolvated crystal of **2**-PMC-I facilitates charge compensation, a behavior similar to that of typical merocyanine aggregates. The packing is such that the molecular dipole moments in relatively closely assembled head-to-tail dimeric PMC units cancel, while short interchain $N^{\delta+}\cdots O^{\delta-}$ contacts help to maintain additional local electrostatic neutrality. By contrast, in the crystalline lattice of **2**-PMC-II, the molecules are more disordered and more loosely packed, which suggests that "self-solvation" may be less important. The presence of polar water molecules contributes to an increase in the effective dielectric of the lattice as well as the clear presence of hydrogen bonding of water molecules to the "phenoxyl" oxygen. Both contributions would be likely to stabilize the zwitterionic resonance contribution, leading to greater stability of the open form and greater zwitterionic character. This result is significant, as it provides the first direct structural evidence for the shift in charge-separated character associated with environment in the crystalline state.

Comparison of the DFT-Optimized Geometries with Experiment. The DFT/B3LYP level of theory has been found to reproduce the experimental geometries of many organic molecules with reasonable accuracies while using a practical level of computational resources,[110,111] and this treatment has been used by several authors in the study of spiropyran and spirooxazine systems.[82,83,112] A comparison of bond lengths predicted by computation to those determined experimentally suggests that DFT reasonably predicts the geometries of the closed forms. DFT geometry optimization calculations for **4**-SO produces bond lengths with an average deviation of 0.006 Å and a maximum deviation of 0.02 Å from those determined experimentally (Table 5, Supporting Information). In particular, the experimental $C_{spiro}-O$ bond lengths are very close to the calculated lengths, which has not always been the case in studies of other spirooxazines.[83,112]

For the open forms **1**-PMC and **2**-PMC, the calculated bond lengths differ more significantly from experiment. Bond lengths in the conjugated azomethine bridge deviate by 0.03−0.05 Å from experiment (Table 6), whereas those in the azahomoadamantyl and phenanthroline groups deviate by 0.01−0.02 Å. The differences between the calculated and experimental bond lengths for the azomethine bridge are greater than the experimental error for crystallographic analysis (the value of 2σ for the XRD measurements is on the order of 0.004−0.020 Å). Deviations of 0.03−0.05 Å are quite significant when one considers that the canonical quinoidal and zwitterionic resonance forms differ only by bond lengths on the order of 0.05−0.10 Å. Importantly, the calculations consistently underestimate the contribution from the zwitterionic resonance form. Furthermore, the DFT-optimized structures possess nearly completely planar bridges (i.e., the α, β, and, γ dihedral angles are $\approx 0°$ or 180°), which does not accurately reflect the slight twisting observed in the crystal structures. From the calculations alone, one would predict a higher contribution from the quinoidal resonance form relative to the zwitterionic form for **1**-PMC and **2**-PMC, which would be misleading in light of the crystallographic data.

Although we cannot compare the calculated geometry for **4**-PMC with experimental crystalline-state structural data, we can analyze the computational results in the context of the solution-state solvatochromism studies. The relative solvatochromic behaviors of **2**-PMC and **4**-PMC suggest that the azahomoadamantyl and indolyl derivatives possess fundamentally different electronic structures, and that the zwitterionic resonance contribution is more substantial in the azahomoada-

(110) Ziegler, T. *Chem. Rev.* **1991**, *91* (5), 651–667.
(111) El-Azhary, A. A.; Suter, H. U. *J. Phys. Chem.* **1996**, *100* (37), 15056–15063.
(112) Minkin, V. I.; Metelitsa, A. V.; Dorogan, I. V.; Lukyanov, B. S.; Besugliy, S. O.; Micheau, J.-C. *J. Phys. Chem. A* **2005**, *109* (42), 9605–9616.

mantyl PMCs. The DFT-optimized geometries for **2**-PMC and **4**-PMC are, however, nearly the same in both the gas phase and more polar media, which does not accurately reflect the differences in electronic structure suggested by the solvatochromism studies.

Thus, both crystalline- and solution-state experiments suggest that the DFT/B3LYP level of theory does not accurately predict the geometries of metastable photomerocyanines. The deviation of the computational geometries from the experimental geometries can be understood within the context of the significant effects of molecular environments on the geometry of the PMC forms. The effect of solvents on solute molecules may be categorized into specific and nonspecific classes, in which nonspecific interactions arise from dispersion and electrostatic interactions between the charge distribution of the solute and solvent molecules. In crystalline **2**-PMC, the crystal packing of the photomerocyanines can be characterized as governed by electrostatic interactions between the charged groups. In **2**-PMC-I, the polar groups are compensated by the close vicinity of the opposite polar groups of neighboring molecules, and in **2**-PMC-II, where the charge compensation is expected to be weaker, by appropriately oriented water molecules leading to stabilization by hydrogen bonding. While electrostatic interactions between solute and solvent can be described by a moment expansion such as that given by Onsager reaction field theory, the addition of an effective dielectric using the Onsager model, even in high dielectric solvents such as DMSO and H_2O, was not found to be sufficient to reproduce experimental geometries of the PMC forms, most likely because of specific and nonspecific intermolecular interactions in the crystalline state. It is well-known that intermolecular interactions may cause the molecular geometries in the crystalline state to be quite different from those of the free molecules,[113,114] e.g., structures of isolated molecules of pyridinium betaines optimized using DFT were found to be significantly different from those observed in the crystals.[115]

In addition to effects due to the specific electronic structures of the PMC forms, there are generalized effects due to computational methodology. Inconsistencies between calculated and experimental geometries are not unexpected given the difficulties in reproducing ground states, excited states, charge-separated states, and acceptor−donor excitations of fully delocalized organic molecules by DFT.[116,117] DFT schemes based on conventional exchange-correlation (XC) functionals have been found to lead to catastrophic values of polarizability and other electronic sructure factors for push−pull conjugated systems. The overly large μ values are associated with an overestimation of the charge transfer between the donor and the acceptor, and incomplete screening of the external electric field is responsible for the large discrepancies. Current XC functionals were found to incorrectly describe the polarization of conjugated systems when the polarization is due to donor−acceptor substitution or an external field or both.[118]

It is clear from the above discussion that DFT displays serious shortcomings in predicting absolute PMC structures as a function of substitution and medium. Discrepancies between calculated and experimental geometries are highly relevant to deriving structure−property relationships in PMCs, because even small changes in electronic structure—as manifested by small changes in molecular geometries—can have significant consequences on the NLO and photochromic properties of these materials. However, calculated and experimental geometries are much more consistent for the SO forms, and DFT may therefore remain a useful tool for predicting structure−property trends for spirooxazines based on SO geometries.

Effects of Molecular Structure on the Charge-Separated Character and Photochromic Properties in Photomerocyanines. To date, the only metastable photomerocyanines that have been structurally characterized are a handful of nitro- and pyridinium-substituted spiropyran or spirothiopyran derivatives, which were all shown to exhibit a predominantly zwitterionic structure in the crystalline state.[38–43] These molecules also display negative solvatochromism, which corroborates their zwitterionic structure in solution.[41,72,119] Only a few permanent spirooxazine-based PMCs have been characterized, and these have been described as predominantly quinoidal in character, in some cases on the basis of the C═O bond length alone.[44,45] Solvatochromic studies of spirooxazine-based PMCs have indicated that these exhibit positive solvatochromic behavior, and it was concluded that they possess a predominantly quinoidal structure.[31,34,68,89] Computational studies have also predicted a quinoidal structure for spirooxazine-based PMCs.[25] The interpretation of these observations—limited to specific derivatives and conditions—led in some instances to ambiguity regarding the nature of the molecular structure of spiropyrans and spirooxazines and,[33,120] in some cases, to the belief that spirooxazines as a class are quinoidal while spiropyrans are zwitterionic.[34] Recently it has been emphasized that the degree of quinoidal or zwitterionic character in these photomerocyanines is a function of substitution pattern and medium.[82] For spirooxazines, recent computational and solvatochromism studies have predicted zwitterionic character in spirooxazine derivatives with electron-withdrawing groups on the oxazine moiety and a dependence of the degree of zwitterionic character on medium polarity.[32] Here, for the first time, we have presented X-ray structural characterization for PMCs of the spirooxazines class, namely, azahomoadamantyl isoquinoline and phenanthroline spirooxazines, and have shown that these derivatives exhibit a predominantly zwitterionic structure in both the crystalline state and in polar solvents.

Trends in the properties of spiropyrans and spirooxazines can be evaluated in terms of the substituents on the amine and oxazine functionalities.[34] Authors have discussed these trends in terms of "donor−acceptor" effects,[82] "push−pull" interactions,[32] or chemical hardness.[121] One of the trends that can be understood in this way is the relative contribution of the charge-separated zwitterionic resonance form to the PMC molecular structure. Because charge separation in these systems results in a greater distribution of positive charge at the amine moiety and of negative charge at the oxazine moiety, the presence of

(113) Hargittai, I. *Pure Appl. Chem.* **1989**, *61* (4), 651–660.
(114) Chiang, J. F.; Song, J. J. *J. Mol. Struct.* **1982**, *96* (1−2), 151–162.
(115) Szafran, M.; Dega-Szafran, Z.; Katrusiak, A.; Buczak, G.; Głowiak, T.; Sitkowski, J.; Stefaniak, L. *J. Org. Chem.* **1998**, *63*, 2898–2908.
(116) Choi, C. H.; Kertesz, M.; Karpfen, A. *J. Chem. Phys.* **1997**, *107* (17), 6712–6721.
(117) Masunov, A. M.; Tretiak, S. *J. Phys. Chem. B* **2004**, *108* (3), 899–907.
(118) Champagne, B.; Perpète, E. A.; Jacquemin, D.; van Gisbergen, S. J. A.; Baerends, E.-J.; Soubra-Ghaoui, C.; Robins, K. A.; Kirtman, B. *J. Phys. Chem. A* **2000**, *104* (20), 4755–4763.
(119) Wojtyk, J. T. C.; Wasey, A.; Kazmaier, P. M.; Hoz, S.; Buncel, E. *J. Phys. Chem. A* **2000**, *104* (39), 9046–9055.
(120) Chibisov, A. K.; Görner, H. *J. Phys. Chem. A* **1999**, *103* (26), 5211–5216.
(121) Domínguez, M.; Rezende, M. C. *J. Phys. Org. Chem.* **2010**, *23* (2), 156–170.

electron-withdrawing groups (EWGs) on the amine would be expected to destabilize the zwitterionic form, while their presence on the oxazine would be expected to stabilize it.[34,82] To date, all of the spiropyran or spirooxazine systems which have been found to exhibit zwitterionic character—as determined by XRD, solvatochromism, or computational studies—are indolyl-based and possess strong EWGs on the oxazine functionality. The substitution of EDGs on the amine does not have a strong enough electronic effect to significantly stabilize the zwitterionic resonance form, at least as predicted by solvatochromism or computational studies (no such PMC derivatives have been structurally characterized). The changes in the electronic structure of the PMC form resulting from the incorporation of the azahomoadamantyl group are apparently much more significant than those resulting from the substitution of EDGs on the amine moiety for typical indolyl derivatives. Whereas the stabilization of the zwitterionic resonance form is typically explained by the delocalization of negative charge onto an electron-withdrawing nitro or pyridinium substituent on the oxazine functionality, this is clearly not the case in the azahomoadamantyl derivatives, in which the zwitterionic form appears to be favored through the stabilization of positive charge by the strongly electron-donating azahomoadamantyl group.

The photochemical and thermal isomerization mechanisms and rates in spirooxazines can be interpreted in the context of their structural features. For the ground-state thermal isomerization process, general consensus is that the SO → PMC isomerization mechanism involves at least a C−O bond cleavage step to form a *cis* intermediate, and a *cis*-to-*trans* isomerization step to form the *trans* PMC isomer.[34,82,83] For the forward SO → PMC thermal isomerization process, the transition states and energy barriers for these steps may be molecular-structure- and medium-dependent. However, the reverse PMC → SO thermal isomerization process is more straightforward to analyze as the rate-limiting step is necessarily *trans*-to-*cis* isomerization, and the rate constant for this process, k_2, can be directly related to the activation energy for bond rotation.[82,83,119] We observed lower k_2 values for the azahomoadamantyl spirooxazines relative to the indolyl spirooxazines. This is consistent with the azahomoadamantyl derivatives having greater zwitterionic character, and therefore a higher bond order for the central C−N bond of the azomethine bridge, which would impede *trans*-to-*cis* isomerization and lead to higher energy barriers for this process.[82,119] The k_2 values were also found to be lower in the isoquinoline spirooxazines relative to the phenanthroline spirooxazines, which suggests that the prior have more zwitterionic character. Finally, the lower k_2 values observed in more polar solvents can be rationalized by a greater stabilization of the PMC form and of the zwitterionic resonance form with increasing solvent polarity. The relative energy difference of the PMC and SO forms ($\Delta E = E_{SO} - E_{PMC}$) as derived from computation [DFT B3LYP/6-31G(d)] for compounds **1**, **2**, and **4** are 20.4, 3.8, and 1.4 kcal/mol, respectively, consistent with stabilization of the open form and increasing rates of PMC → SO conversion (k_2) along the series. All of the structural features highlighted here are consistent with the XRD and solvatochromism studies described above.

The degree of quinoidal or zwitterionic character in PMCs can also be correlated with the structure of the SO form. Those structurally characterized PMCs which have strong EWGs on the oxazine moiety and exhibit zwitterionic character also tend, in the SO form, to have C_{spiro}−O bond lengths at the upper limit of those found for spirooxazines in general.[42] The azahomoadamantyl derivatives **1** and **2** are no exception to this trend, and exhibit particularly long C_{spiro}−O bond lengths. However, whereas for previously reported spirooxazines, these long bonds could be explained by a stronger anomeric effect caused by a greater removal of electron density from the oxygen atom due to EWGs on the oxazine moiety, for the azahomoadamantyl derivatives they can instead be explained by the greater availability of the lone pair on the nitrogen atom as a result of the electron-donating properties of the amine functionality. As regards photochromic properties, long spirooxazine C_{spiro}−O bond lengths are expected to lead to lower activation energies for the initial bond cleavage step, both thermally and photochemically, though this may not be the most important step in determining forward thermal isomerization rates or photocoloration quantum yields.[82,122]

Conclusions

We have presented investigations of medium and substitution effects on the molecular structure of photomerocyanines of the spirooxazines class. The structural features examined here suggest that bicyclic azahomoadamantyl substitution leads to significant stabilization of the zwitterionic resonance form without destroying photochromic activity. A comparison of the vibrational structure and solvatochromism of the PMC $\pi-\pi^*$ absorption band of the indolyl and azahomoadamantyl derivatives suggests that the two families have fundamentally different ground-state structures, where the indolyl derivatives have more quinoidal character in a medium of given polarity. The two spirooxazine families exhibit different ranges of accessible quinoidal/zwitterionic resonance contributions; even in very high polarity solvents, the indolyl derivatives do not show negative solvatochromic evidence of zwitterionic character, while the azahomoadamantyl derivatives exhibit negative solvatochromism in both hydrogen-bond donating and non-hydrogen-bond donating polar solvents. The electronic properties observed in the azahomoadamantyl derivatives are consistent with the amine functionality acting as a very strong electron-donating group. Azahomoadamantyl derivatization is therefore a synthetically feasible and potentially powerful approach to designing spirooxazines in which the PMC isomer has significant charge-separated character and associated photochromic properties such as slow thermal back reactions.

The XRD analysis of metastable photomerocyanines from the spirooxazine class of photochromic molecules in azahomoadamantyl isoquinoline and phenanthroline derivatives indicates a substantial contribution from the canonical zwitterionic resonance form in the crystalline state. A comparison of the XRD and solvatochromism for the azahomoadamantyl PMCs suggests that because a quinoidal structure is inferred from solution studies in nonpolar solvents, yet a predominantly zwitterionic structure is evident in the crystalline state, the crystal lattice may act as a strong dielectric medium. A shift in the bond-length alternation of the azomethine bridge in two pseudopolymorphs of **2**-PMC suggests that changes in specific intermolecular interactions and dielectric of the crystalline lattice affect the relative contributions of the quinoidal and zwitterionic resonance forms. These results have important implications for the sensitivity of charge-separated states to their environment in constrained media. Finally, the direct XRD evidence for the

(122) Maurel, F.; Aubard, J.; Millie, P.; Dognon, J. P.; Rajzmann, M.; Guglielmetti, R.; Samat, A. *J. Phys. Chem. A* **2006**, *110* (14), 4759–4771.

structures of the metastable spirooxazine-based PMCs reported here, in combination with the investigation of medium polarity effects on PMC structure in both the crystalline and solution states, may lead to a better understanding of medium effects and structural features governing the degree of charge-separation in organic systems.

Experimental Section

Spectroscopic Methods. All electronic absorption spectroscopy was performed with an Agilent 8453 spectrometer. For the photoisomerization experiments, solutions were prepared at concentrations of $10^{-5}-10^{-6}$ M in spectrograde solvents. The samples were exposed to steady-state irradiation from a high-pressure Hg arc lamp operating at 60 W with glass cutoff filters to obtain the desired wavelength range ($280 < \lambda < 400$ nm for UV irradiation, and $\lambda > 500$ nm for visible irradiation). The observed rate constants of thermal reversion were determined in the absence of light by following the absorbance kinetics at λ_{max} after generating a photostationary state, and fitting the data to monoexponential rate functions by linear least-squares methods. Runs were repeated several times and averaged for accuracy.

Computational Methods. Geometry optimization calculations were performed using density functional theory (DFT) with the hybrid Becke-style three-parameter exchange functional[123] and the Lee−Yang−Parr correlation functional[124] (B3LYP) with the Gaussian 03 software package.[125] The optimization for **3**-PMC was performed from a starting geometry based on the X-ray diffraction analysis atomic coordinates. Solvent effects were modeled in toluene ($\varepsilon = 2.379$), DMSO ($\varepsilon = 46.7$), and H_2O ($\varepsilon = 78.39$) using the Onsager model with a_o values of 5.64 Å for **2**-PMC and 5.95 Å for **4**-PMC as determined by a volume calculation in Gaussian. Stability calculations were performed on all optimized geometries obtained from gas-phase calculations, and structures were found to be minima on the potential energy surfaces.

Synthesis of Spirooxazines. Compounds **1**,[46] **4**,[19] **6**,[63] **7**,[64] **9**,[65] **10**,[66] **12**,[67] and **13**[67] were prepared according to previously reported procedures and characterized by ^{1}H NMR spectroscopy and/or melting points (Supporting Information). The ^{1}H NMR spectra of **2** and **3** were assigned with COSY and NOESY spectroscopy and are labeled according to the connecting carbon atoms (see Figures 5 and 7 for atom numbering).

4-Methylspiro[4-azahomoadamantane-5,2′-[2*H*-1,4]oxazino-[2,3-*f*][1,10]phenanthroline] {Spiro[azahomoadamantane-phenanthrolinoxazine] (2)}. Et_3N (1.60 mL, 11.5 mmol) was added to a stirring solution of 4,5-dimethyl-4-azahomoadamant-4-enium iodide (**13**) (1.72 g, 5.62 mmol) in CH_2Cl_2 (150 mL) at 0 °C. After 30 min, 4 Å molecular sieves (∼3 g) and 5-hydroxy-6-nitroso-1,10-phenanthroline (**10**) (1.27 g, 5.63 mmol) were added to the mixture, and the solution was slowly warmed to rt and then heated at reflux for 3 h. The solution was filtered, washed with $NaHCO_3$, H_2O, and brine, and then dried over $MgSO_4$, before removal of the solvent by rotary evaporation to yield a dark purple solid (1.4 g, 65% yield) of reasonable purity. The material was further purified by column chromatography on silica gel with CH_2Cl_2/CH_3OH (90:10) followed by recrystallization from EtOAc to yield iridescent green crystals (0.69 g, 32% yield). Mp: 200−201 °C. ^{1}H NMR (300 MHz, $CDCl_3$) PMC form: δ 9.97 (s, 1H, H-3), 9.03 (dd, J = 4.5, 1.7 Hz, 1H, H-24), 8.75 (dd, J = 7.9, 1.7 Hz, 1H, H-22), 8.74 (dd, J = 4.4, 2.1 Hz, 1H, H-21), 8.64 (dd, J = 8.1, 2.2 Hz, 1H, H-19), 7.48 (dd, J = 8.1, 4.4 Hz, 1H, H-23), 7.39 (dd, J = 8.0, 4.4 Hz, 1H, H-20), 5.11 (tt, J = 5.9, 1.9 Hz, 1H, H-10), 3.74 (septet, J = 2.1 Hz, 1H, H-6), 3.51 (s, 3H, H-1), 2.20−1.75 (m, 12H); SO form: δ 9.14 (dd, J = 4.5, 2.1 Hz, 1H, H-24), 8.86 (dd, J = 8.1, 1.4 Hz, 1H, H-19), 7.63 (dd, J = 8.1, 4.4 Hz, 1H, H-23), 7.61 (dd, J = 8.1, 4.4 Hz, 1H, H-20), 7.70 (s, 1H, H-3), 2.47 (s, 3H, H-1), 2.20−1.75 (m, 12H) ppm (the remaining signals for the SO form are not distinguishable from those of the PMC form). ^{13}C NMR (125 MHz, $CDCl_3$) PMC and SO forms: δ 179.5 (C), 174.5 (C), 157.36 (CH), 152.6 (CH), 151.2 (C), 150.4 (CH), 147.8 (CH), 146.8 (CH), 146.4 (C), 143.5 (C), 140.1 (C), 135.2 (CH), 133.1 (C), 130.9 (CH), 130.4 (CH), 129.9 (CH), 129.7 (C), 127.8 (C), 127.1 (C), 125.9 (CH), 123.5 (CH), 123.3 (CH), 122.9 (CH), 122.7 (CH), 122.1 (C), 119.4 (C), 95.2 (C), 77.2 (C/CH), 64.5 (CH), 58.9 (CH), 42.9 (CH), 39.8 (CH_2), 39.7 (CH_2), 39.4 (CH_2), 38.4 (CH_2), 36.0 (CH_2), 34.0 (CH_2), 33.9 (CH_2), 33.6 (CH_2), 32.3 (CH_2), 30.2 (CH_2), 30.0 (CH_2), 29.3 (CH/CH_3), 26.7 (CH/CH_3), 26.7 (CH/CH_3), 26.2 (CH/CH_3) ppm. EI-MS: *m*/*z* (%) 384 (91) $[M]^+$, 163 (100). Anal. Calcd for $C_{24}H_{24}ON_4$: C, 74.98; H, 6.29; N, 14.57. Found: C, 74.71; H, 6.17, N, 14.36.

1,3-Dihydro-1,3,3-trimethylspiro[2*H*-indole-2,3′-[3*H*]pyrido-[3,4-*f*][1,4]benzoxazine] {Spiro[indoline-isoquinolinoxazine] (3)}. [126] 7-Hydroxy-8-nitrosoisoquinoline (**7**) (206 mg, 1.18 mmol) and 1,3,3-trimethyl-2-methylene indoline (**15**) (0.209 mL, 1.18 mmol) were heated at reflux in 2-propanol (30 mL) over 4 Å molecular sieves for 3.5 h. The solvent was removed by rotary evaporation, and the material was purified by column chromatograph on silica gel first with CH_2Cl_2/CH_3OH (95:5) and then with EtOAc/hexanes (40:60). Recrystallization from EtOAc yielded yellow crystals (136 mg, 35% yield). Mp: 163−164 °C. ^{1}H NMR (360 MHz, $CDCl_3$): δ 9.95 (t, J = 0.8 Hz, 1H, H-19), 8.49 (d, J = 5.7 Hz, 1H, H-20), 7.80 (s, 1H, H-3), 7.62 (br d, J = 8.9 Hz, 1H, H-16), 7.53 (dd, J = 5.7, 0.8 Hz, 1H, H-21), 7.21 (td, J = 7.8, 1.3 Hz, 1H, H-13), 7.20 (d, J = 8.8 Hz, 1H, H-15), 7.08 (dd, J = 7.3, 1.1 Hz, 1H, H-11), 6.90 (td, J = 7.3, 0.8 Hz, 1H, H-12), 6.57 (br d, J = 7.8 Hz, 1H, H-14), 2.75 (s, 3H, H-1), 1.36 (s, 3H, H-7/H-8), 1.34 (s, 3H, H-7/H-8) ppm. ^{13}C NMR (90 MHz, $CDCl_3$): δ 152.4 (Ar CH), 147.3 (Ar CH), 144.5 (Ar C), 141.9 (Ar CH), 135.6 (Ar C), 131.4 (Ar C), 128.7 (Ar CH), 128.1 (Ar CH), 125.1 (Ar C), 123.0 (Ar C), 121.6 (Ar CH), 121.5 (Ar CH), 120.0 (Ar CH), 119.9 (Ar CH), 107.2 (CH), 99.0 (C), 77.2 (C), 52.0 (C), 29.6 (CH_3), 25.4 (CH_3), 20.7 (CH_3) ppm. EI-MS: *m*/*z* (%) 329 (57) $[M]^+$, 314 (60), 159 (100), 144 (41). Anal. Calcd for $C_{21}H_{19}N_3O$: C, 76.57; H, 5.81; N, 12.76. Found: C, 76.81; H, 5.91, N, 12.50.

Acknowledgment. The authors thank the American Chemical Society Petroleum Research Fund (ACS-PRF), the British Columbia Knowledge Development Fund (BCKDF), the Canada Foundation for Innovation (CFI), the Natural Sciences and Engineering Council of Canada (NSERC), the University of Victoria, and the University of Washington for financial support of this research. M.M.P. thanks NSERC for an NSERC-CGS fellowship and PEO International for a PEO Scholar Award.

Supporting Information Available: Characterization of compounds by NMR, packing diagrams and geometric parameters from XRD analysis, crystallographic data and cif files, electronic absorption spectroscopy of **1** in representative solvents, details of spectral deconvolution for **2** and **4**, concentration dependence studies for **2** and **4**, theoretical and experimental determination of ^{1}H and ^{13}C NMR shifts of **2** and **4**, complete ref 125, basis set comparison, and Gaussian outputs. This material is available free of charge via the Internet at http://pubs.acs.org.

JA100238H

(123) Becke, A. D. *J. Chem. Phys.* **1993**, *98* (7), 5648–5652.
(124) Lee, C. T.; Yang, W. T.; Parr, R. G. *Phys. Rev. B* **1988**, *37* (2), 785–789.
(125) Frisch, M. J.; et al. *Gaussian 03*, Revision E.01; Gaussian, Inc.: Wallingford CT, 2004.
(126) Salemi-Delvaux, C.; Giusti, G.; Guglielmetti, R.; Dubest, R.; Aubard, J. *J. Chim. Phys. Phys.-Chim. Biol.* **1998**, *95* (9), 2001–2014.